AGU PUBLICATIONS

JGR

Journal of Geophysical Research: Solid Earth

RESEARCH ARTICLE
10.1002/2017JB013991

Key Points:
- 3-D modeling shows double subduction of an oceanic plate led to arc-arc collision in the Molucca Sea region
- Observed slab shape, migration, and deformation of arcs are reproduced by asymmetrical subduction
- Toroidal flow is crucial for escape of slab-trapped mantle and confines DDS to narrow and short oceanic plate

Supporting Information:
- Supporting Information S1
- Movie S1
- Movie S2
- Movie S3
- Movie S4
- Movie S5

Correspondence to:
F. Guo,
guofengt@263.net

Citation:
Zhang, Q., F. Guo, L. Zhao, and Y. Wu (2017), Geodynamics of divergent double subduction: 3-D numerical modeling of a Cenozoic example in the Molucca Sea region, Indonesia, *J. Geophys. Res. Solid Earth*, *122*, 3977–3998, doi:10.1002/2017JB013991.

Received 19 JAN 2017
Accepted 17 APR 2017
Accepted article online 20 APR 2017
Published online 12 MAY 2017

Geodynamics of divergent double subduction: 3-D numerical modeling of a Cenozoic example in the Molucca Sea region, Indonesia

Qingwen Zhang[1,2], Feng Guo[1], Liang Zhao[1], and Yangming Wu[1,2]

[1]State Key Laboratory of Isotope Geochemistry, Guangzhou Institute of Geochemistry, Chinese Academy of Sciences, Guangzhou, China, [2]College of Earth Sciences, University of Chinese Academy of Sciences, Beijing, China

Abstract Geological observations reveal existence of a unique form of plate subduction featuring subduction on both sides of one single oceanic plate, which is termed divergent double subduction (DDS). DDS may play an important role in facilitating tectonic processes like closure of oceanic basins, accretion and amalgamation of magmatic arcs, and growth of continents. However, this type of subduction has been largely a conceptual model and the geodynamics behind DDS are still poorly constrained. The Molucca Sea subduction zone in SE Asia has been considered as a Cenozoic example of DDS based on geophysical and geological data and provides an opportunity for detailed assessment of how DDS occurs. Here we present 3-D numerical modeling with aims to reproduce the geodynamic processes of DDS. Several factors that may have important influences on the evolution of DDS are evaluated, including the geometry of the subducting plate, the order of subduction initiation on both sides, the far-field boundary conditions and thickness of the overriding plates, and the negative buoyancy of the subducting plate. Our results reproduce the observed asymmetrical shape of the subducting Molucca Sea plate and the bending of Halmahera and Sangihe arcs and suggest that DDS is possible if effective escape of the slab-trapped upper mantle overcomes the space problem, otherwise the slab-trapped mantle may hinder the sustainability of subduction. We therefore conclude that DDS is associated with closure of narrow and short oceanic plate, and large-scale double subduction is rare in nature probably owing to space problem.

Plain Language Summary Divergent double subduction (DDS) is a potential way for closure of oceanic basins in plate tectonics, but its mechanism remains unsolved. The Molucca Sea subduction zone in SE Asia is a unique Cenozoic example of DDS. In this study, we present 3-D numerical modeling of how DDS occurs. Our results reproduce the observed asymmetrical inverted U shape of the subducting Molucca Sea plate and the bending of Halmahera and Sangihe arcs and suggest that DDS is possible if effective escape of the slab-trapped upper mantle overcomes the space problem, otherwise the slab-trapped mantle may hinder the sustainability of subduction. We therefore conclude that DDS is associated with closure of narrow and short oceanic plate, and large-scale double subduction is rare in nature probably due to the space problem. Our results provide important geodynamic constraints on tectonic processes in association with DDS, such as closure of the oceanic basins, collision between magmatic arcs, and continental growth in plate margins.

1. Introduction

Subduction of oceanic plates is the most important process for mass and energy exchange between Earth's surface and interior. Subduction results in diverse types of tectonic movements, and slab pull due to descent of cold and dense oceanic lithosphere has been considered to be the dominant driving force of plate tectonics [e.g., *Forsyth and Uyeda*, 1975; *Cloos*, 1993; *Conrad*, 2002; *Turcotte and Schubert*, 2014; *Seton et al.*, 2015]. In general, an oceanic lithosphere is consumed on one side of a plate as it subducts, while the other side borders another plate at a mid-oceanic ridge (e.g., the Pacific plate). Subduction leads to formation and migration of magmatic arcs, opening of back-arc basins, fragment of continents, or accretion of crustal fragments [e.g., *Rey and Müller*, 2010; *Gerya and Meilick*, 2011; *Moresi et al.*, 2014; *Capitanio et al.*, 2015]. Interactions between the subducting slab, the overriding plate, and the ambient upper mantle are also responsible for magmatism, metamorphism, and earthquake activity at subduction zones [e.g., *Gutscher et al.*, 2000; *Liu and Stegman*, 2012; *Pownall et al.*, 2013; *Bouilhol et al.*, 2015; *Ji et al.*, 2016]. Subduction may also occur on both sides of a single oceanic plate, promoting closure of an oceanic basin and leading to

convergence and collision of the overriding plates. Therefore, this type of subduction, termed divergent double subduction (DDS) [*Soesoo et al.*, 1997], could have played an important role in tectonic evolution in geologic history. *Soesoo et al.* [1997] proposed that the Silurian to Early Carboniferous granitoids and later bimodal magmatism in the Lachlan fold belt, SE Australia, were a likely consequence of DDS. Symmetrical and contemporaneous assemblages of volcanic arcs led *Zhao* [2015] to propose double subduction of an oceanic lithosphere during the Neoproterozoic convergence between the Yangtze and Cathaysian blocks in the Jiangnan Orogen, SE China. The distribution of Paleozoic subduction-accretion complexes and magmatic arcs of similar age on both sides of the Solonker suture zone also suggested likely occurrence of DDS, which led to convergence between the Mongolian block and North China craton and final closure of the Paleo-Asian Ocean during Late Permian to Early Triassic [*Xiao et al.*, 2003, 2015; *Eizenhöfer et al.*, 2014]. These old geological records are usually too incomplete to constrain the evolution of DDS, and young cases are required to provide better insights into this unique form of subduction. The Cenozoic had witnessed spectacular regional tectonic activities between the Tethys and the western Pacific since the Mesozoic breakup of the Gondwana supercontinent. These tectonic movement involved westward subduction of the Pacific plate, northward migration of the Indian and Australian continents, and opening of many back-arc basins along the Eurasian margin [*Maruyama et al.*, 1997; *Hall and Spakman*, 2002; *Schellart et al.*, 2006; *Hall*, 2012; *Morley*, 2012]. A Cenozoic sample of DDS is observed in the Mediterranean region, in which double subduction of the Adria microplate occurred on its eastern and western sides [e.g., *Devoti et al.*, 2002; *Faccenna and Becker*, 2010]. Numerous examples of ongoing tectonic processes like back-arc extension, migration, and accretion of magmatic arcs can also be observed in the Cenozoic subduction zones of SE Asia and the western Pacific. Here we focus on another important example of DDS from the Molucca Sea subduction zone in eastern Indonesia, based on previous geophysical and geological data [*Silver and Moore*, 1978; *McCaffrey et al.*, 1980; *Puspito et al.*, 1993; *Widiyantoro and Hilst*, 1997; *Rangin et al.*, 1999; *Hall*, 2002, 2012; *Hall and Spakman*, 2015] (Figures 1–3). Subduction of the Molucca Sea plate in the form of DDS provides insights into the geodynamics of arc-arc collision, the causes of magmatic and seismic activities, and the evolution of ancient subduction.

From observations of ancient and Cenozoic examples, it is likely that DDS may have occurred many times during closure of oceanic basins in which there have been complex interactions between the subducting plates, overriding plates and mantle. However, despite its potential importance in plate tectonics, DDS was largely a conceptual model until recent 3-D modeling study revealed an escape pattern of mantle flow induced by subduction of a narrow oceanic plate [*Di Leo et al.*, 2014]. The driving mechanism and factors that may influence the development of DDS remain poorly constrained. It is also interesting that single-sided subduction, rather than DDS, is the dominant type of subduction. The reason for this rarity of DDS is also worthy of further investigations.

In this study, we present 3-D numerical modeling of DDS mainly relevant to the Cenozoic tectonic evolution in the Molucca Sea region, which features convergence and collision between the Sangihe and Halmahera arcs and has global significance in plate tectonics. Potentially important geometric and rheological configurations are tested in different numerical models to reproduce morphological and geophysical features of the present-day Molucca Sea region. Results are in good agreement with these key geophysical observations of this region and thus provide important geodynamic constraints on tectonic processes in association with DDS, such as closure of oceanic basins, collision between magmatic arcs and continental growth.

2. Cenozoic Molucca Sea Subduction Zone

Numerous marginal seas, small oceanic basins and magmatic arcs exist in the vast region between the western Pacific and the Indo-Australian plates, with their formation linked to westward subduction of the Pacific plate and northward subduction of the Australian plate into a unique region of mantle described as "slab-graveyards" [*Maruyama et al.*, 2007] (Figures 1–3). In eastern Indonesia, tectonic evolution features complex accretion of microplates onto surrounding major plates and opening of small oceanic basins, including arc-arc collision in response to subduction of the Molucca Sea plate and convergence between the Eurasian and Philippine Sea plate (Figure 3) [*McCaffrey et al.*, 1980; *Hall*, 1987, 1996, 1997; *Hinschberger et al.*, 2005]. Geological and geophysical data indicate occurrence of DDS in the Molucca Sea region, which may have affected tectonic evolution of surrounding regions, such as the Banda Sea region [*Milsom*, 2001]. Seismic

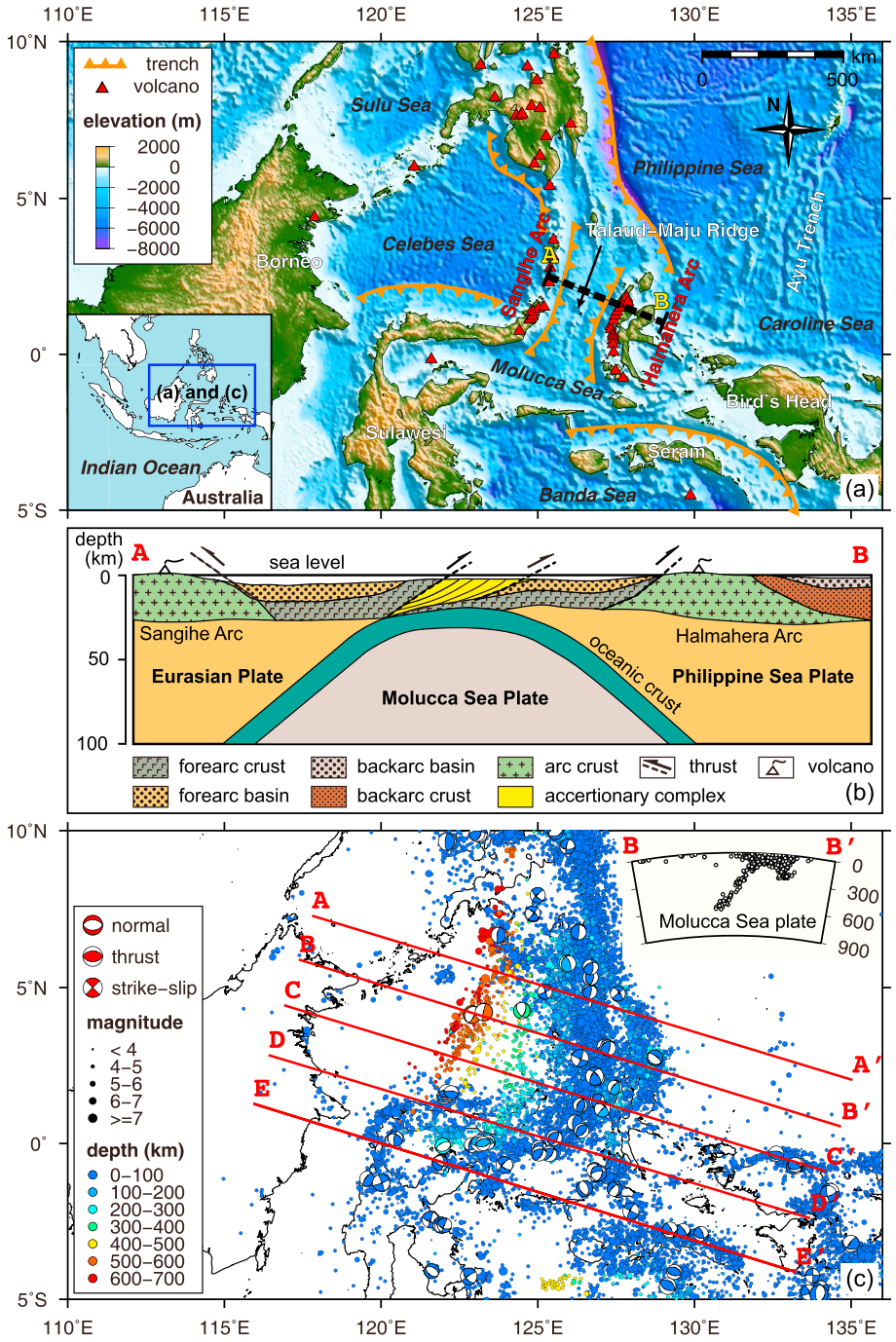

Figure 1. (a) Sketch of the Molucca Sea subduction zone and its vicinity. (b) Cross section (A-B) demonstrating the structure of arc-arc collision zone (modified after *Hall and Smyth* [2008]). (c) Distribution of earthquake events (2011.1.1–2015.12.31) and focal mechanism; the insert shows the vertical profile of epicenters sliced at position B-B′. The black dashed line in Figure 1a is the position of cross section A-B in Figure 1b, and the red solid lines in Figure 1c are the cross sections of the seismic tomographic velocity model in Figure 2. The global relief model ETOPO1 is used, and earthquake events are from the U.S. Geological Survey website (http://earthquake.usgs.gov/earthquakes/search/) and the focal mechanisms from GCMT catalog (http://www.globalcmt.org).

reflection, refraction and gravity profiles reveal widespread overthrusting of accretionary complexes onto the fore-arc sedimentary basins of the adjacent Sangihe and Halmahera arcs and have been interpreted as a consequence of collision between the Eurasian and the Philippine Sea plates [*Silver and Moore*, 1978; *McCaffrey et al.*, 1980; *Hall and Smyth*, 2008] (Figure 1b). Following complete subduction of the Molucca

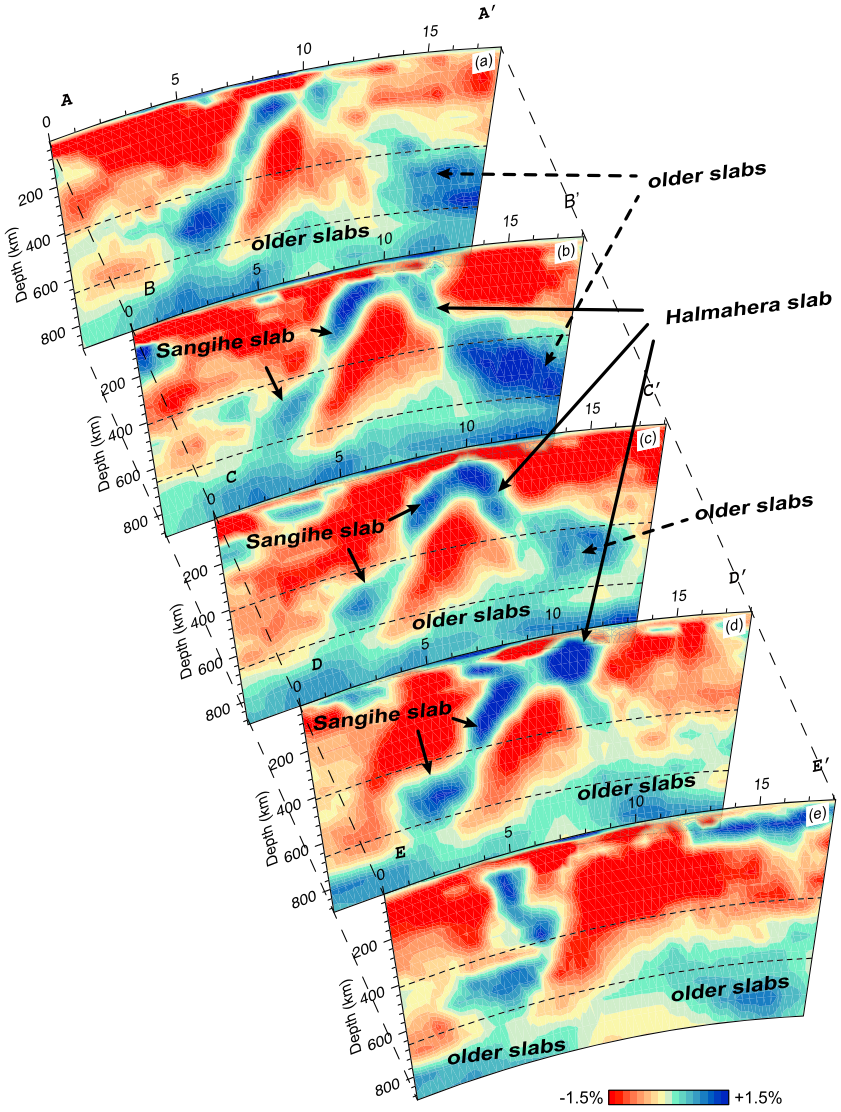

Figure 2. Vertical slices of seismic velocity beneath the Molucca Sea and its surrounding regions, in which positive velocity anomalies outline the unique shape of the subducting Molucca Sea plate. The tomographic images are sliced from the global *P* wave velocity anomaly model *UU-P07* [*Amaru*, 2007] along positions shown in Figure 1c.

Sea plate, the final collision between the overriding Eurasian and the Philippine Sea plates also leads to exhumation of the fore-arc crust, uplift of the Talaud-Maju ridge at the center of the Molucca Sea, and bending of the Sangihe and Halmahera arcs (Figure 1a). Accurate positioning of earthquakes reveals an asymmetrical inverted U shape of a plate beneath the Molucca Sea region (Figure 1c). This is in agreement with the shape of the subducted Molucca Sea plate identified by *P* wave seismic tomography (Figure 2), with the west dipping Sangihe slab having been subducted more deeply than the east dipping Halmahera slab. The trenches are buried by an accretionary complex at shallow depth [*Silver and Moore*, 1978; *Puspito et al.*, 1993; *Widiyantoro and Hilst*, 1997; *Hall*, 2002; *Hall and Spakman*, 2015]. The western Sangihe slab has been subducted as far as the 660 km discontinuity between the upper and lower mantle, whereas the eastern Halmahera slab has reached a depth of 350–400 km. Both slabs dip at angles of ~45°. It is estimated that the total length of the seismically active Molucca Sea plate is 1400–1600 km, 900 km of which was subducted under the Sangihe arc and ~450 km under the Halmahera arc [*Hall and Spakman*, 2015] (Figures 1c and 2). By means of shear wave splitting measurement, mantle flow pattern in response to subduction of the Sangihe and Halmahera slabs was inferred in this region, indicating lateral escape of mantle beneath the Molucca Sea plate [*Di Leo et al.*, 2012, 2014].

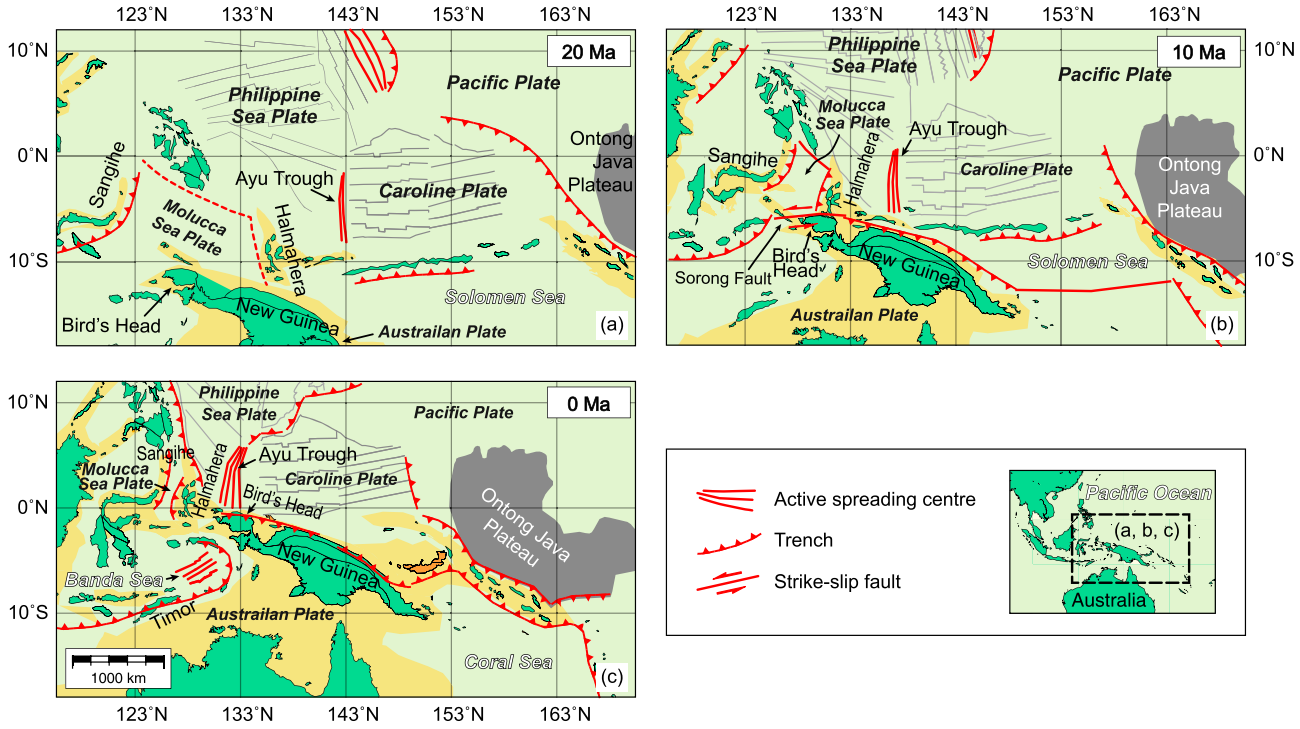

Figure 3. Schematic restruction of tectonic evolution in the SE Asia and western Pacific at (a) 20 Ma, (b) 10 Ma, and (c) 0 Ma. Modified after *Hall* [2002], *Gaina and Müller* [2007], and *Seton et al.* [2012].

3. Model Setup

3.1. Governing Equations

Modeling is performed by solving Stokes equations for steady incompressible creeping flow. We have the mass conservation equation

$$\nabla \cdot u = 0 \tag{1}$$

and momentum conservation equation

$$\frac{\partial \sigma'_{ij}}{\partial x_j} - \frac{\partial p}{\partial x_i} + \rho g_i = 0 \tag{2}$$

where u is the velocity, p is the pressure, $g = 9.8$ m/s^2 is the gravitational acceleration, σ'_{ij} is the deviatoric stress tensor, and for incompressible flow we have

$$\sigma'_{ij} = 2\eta\dot{\varepsilon}_{ij} = \eta\left(\frac{\partial u_i}{\partial x_j} + \frac{\partial u_j}{\partial x_i}\right) \tag{3}$$

where $\dot{\varepsilon}_{ij}$ is the strain rate, subscripts i and j denote the index of spatial coordinates. The thermal effects on DDS subduction are neglected in this study for simplicity due to relatively short duration of modeling that lasts less than 50 Ma.

The geodynamic code Underworld [*Moresi et al.*, 2003, 2007] is used to solve the Stokes equations, which is a parallel software framework based on Lagrangian particle-in-cell finite element scheme and is capable of 2-D/3-D thermal-mechanical-chemical modeling of tectonic processes including mantle convection, subduction of plates and continental collision.

3.2. Geometry and Rheology

We choose a 3-D Cartesian box 3200 km in length, 660 km in depth and 2000–4000 km in width (see Figure 4 and Table 1 for details) to mimic the upper mantle into which the plate sinks in response to gravitational instability between the dense oceanic plate and the ambient mantle material.

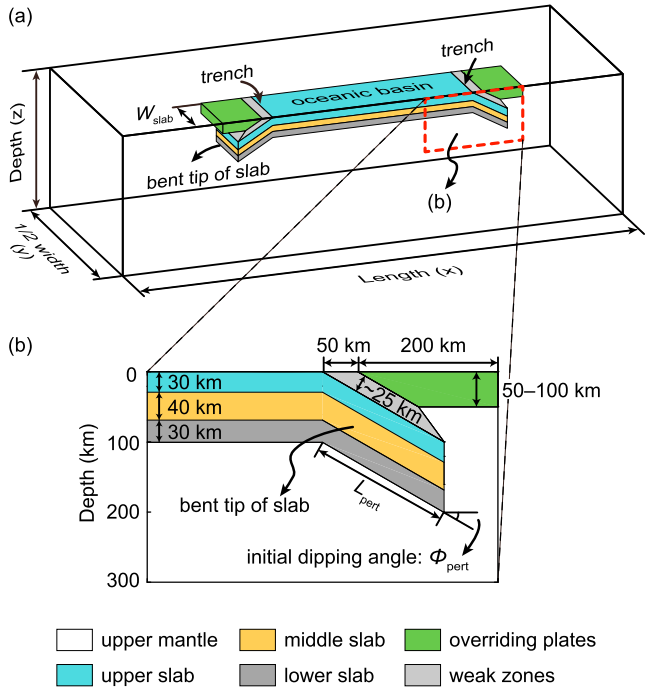

Figure 4. Model setup shown in (a) oblique view and (b) enlarged side view of the slab hinge region. The domain is a Cartesian box with dimensions of 3200 km (length) × 1000–2000 km (half width) × 660 km (thickness or depth). The presubduction slab is divided into the top, middle, and bottom layers with thicknesses of 30, 40, and 30 km, respectively. This plate is flanked by two preexisting bent tips (i.e., the initial bent part of the oceanic plate) used to trigger subduction, with varied initial lengths (L_{pert}) of 150–200 km and dipping angles (φ_{pert}) of 20°–30°. The overriding plates are above the subduction zones at both side of the plate. Two weak zones with identical density and viscosity with that of the upper mantle are also used to enhance decoupling between the overriding plates and the subducting plate.

The oceanic plate is assumed to have a highly simplified triple-layered structure with a viscoplastic top layer and viscous middle and bottom layers with thicknesses of 30, 40 and 30 km, respectively [*Capitanio et al.*, 2009]. For the top viscoplastic layer, von Mises yield criterion is employed with cohesion of 30 MPa and initial viscosity of $1000 \times \eta_{um}$, and when yield occurs, the effective viscosity is replaced by

$$\eta_{eff} = \frac{\sigma_{yield}}{2\dot{\varepsilon}_{II}} \quad (4)$$

where σ_{yield} is the cohesive strength and $\dot{\varepsilon}_{II} = \sqrt{1/2\dot{\varepsilon}_{ij}\dot{\varepsilon}_{ij}}$ is the second invariant of the deviatoric strain rate. The density of subducting plate is laterally uniform and is 40–80 kg/m^3 denser than the ambient upper mantle [*Cloos*, 1993; *Korenaga and Korenaga*, 2016]. This structure mimics the nature of normal mature oceanic lithosphere, which becomes dense enough to subduct due to cooling and mineral phase transformation if the oceanic lithosphere is older than ~30 Myr [*Korenaga and Korenaga*, 2016], facilitating subduction when the topmost viscoplastic layer yields and weakens. DDS is triggered by two bending tips of the presubducting plate at both sides (Figure 4), each with initial lengthes of 150–200 km and dipping angles of 20°–30°, depending on configuration for specific models. The capability of yielding and weakening of the topmost slab layer is the key to sustainable subduction [e.g., *Capitanio et al.*, 2009, 2010; *Stegman et al.*, 2010; *Moresi et al.*, 2014]. Two weak zones, which are assumed to be preexisting faults with identical viscosity and neutral-buoyancy relative to the upper mantle, are also used to facilitate the decoupling between the subducting slabs and overriding plates at the initial stage of subduction. The overriding plates with the same width as the

Table 1. Key Parameters of Geometry and Rheology for the Reference Model (DDS_Ref)

	Size ($L \times H \times W$, km)[a]	Density ($\Delta\rho$)[b]	Viscosity[b]	Tip Dipping Angle	Tip Length
Entire domain	3200 × 660 × 2000	–	–	–	–
Upper mantle	3200 × 660 × 2000	0 kg/m^3	η_{um}	–	–
Upper slab[c]	1000 × 30 × 600	60 kg/m^3	$1000 \times \eta_{um}$	30°	200 km
Middle slab	1000 × 40 × 600	60 kg/m^3	$700 \times \eta_{um}$	30°	200 km
Lower slab	1000 × 30 × 600	60 kg/m^3	$70 \times \eta_{um}$	30°	200 km
Overriding plates[d]	200 × 50 × 600	0 kg/m^3	$200 \times \eta_{um}$	–	–

[a] L, H, and W refer to length, thickness (or depth) and width defined in direction as showing in Figure 4. Only half of the domain along width direction is actually modelled (see Figure 4a).
[b] The values of density and viscosity are presented in this paper as the differences from those of the upper mantle (ρ_{um} = 3200 kg/m^3 and $\eta_{um} = 2.0 \times 10^{20}$ Pa s).
[c] The viscoplastic upper layer of slabs has cohesion of 30 MPa with von Mises yield criterion employed.
[d] We assume that the overriding plates are of neutral buoyance and stronger with respect to the upper mantle. Length of the overriding plates is gauged at surface.

Table 2. Models Designed With Respect to the Reference Model DDS_Ref

Model	Description of Variable	Symbol	Value
DDS_W200	slab width	W_{slab}	200 km
DDS_W600	slab width	W_{slab}	600 km
DDS_W1000	slab width	W_{slab}	1000 km
DDS_W2000	slab width	W_{slab}	2000 km
DDS_30–20	initial dipping angles of bent tips of slabs (left, right)	φ_{pert}	30°, 20°
DDS_200–150	initial lengths of bent tips of slabs (left, right)	L_{pert}	200 km, 150 km
DDS_CBL100	thickness of overriding plate on the left	H_{cbl}	100 km
DDS_Fixed	fix one side of the overriding plate[a]	–	–
DDS_Ref_2D[b]	2-D version of DDS_Ref	–	–
DDS_30-20_2D[b]	2-D version of DDS_30-20	–	–
DDS_200-150_2D[b]	2-D version of DDS_200-150	–	–
DDS_Δρ40	density contrast of slab	$\Delta\rho$	40 kg/m^3
DDS_Δρ80	density contrast of slab	$\Delta\rho$	80 kg/m^3

[a]The overriding plate is fixed to the sidewall by setting far-field boundary, which is in turn controlled by its width. If an overriding plate is attached to this boundary and cannot drift horizontally, it is imposed a "fixed" far-field boundary or a "free" far-field boundary that allows free motion if exerted external force.
[b]These 2-D models are simplified from their 3-D equivalences without considering the third trench-parallel dimensional. A 2-D DDS model is thus equivalent to a 3-D one with infinite width of slab and eliminates toroidal mantle flow. Huge computations required to run very wide 3-D models are avoided with this simplification.

subducting plate are placed at both sides of the oceanic plate above the perturbed slab tips. The viscosity of the mantle, the overriding plates, and the subducting plate are assumed to be Newtonian, and the values remain constant during DDS, with the exception of the topmost slab layer, the viscosity of which decreases when yielding occurs (Figure 4 and Table 1). It is more realistic that the upper mantle is a non-Newtonian fluid and its rheology is dependent on strain, temperature, pressure, and presence of volatiles [e.g., *Karato and Wu*, 1993; *Hirth and Kohlstedt*, 2003]. Variations of these parameters can lead to complex feedback of the upper mantle's rheology and the subduction geodynamics further [e.g., *Jadamec and Billen*, 2010, 2012]. However, because the time scale of modeling is relatively short (less than 30 Ma for most of the models), the influences of these variations are neglected. This is an acceptable compromise in order to avoid bringing in too much uncertainty by reducing these independent variables [e.g., *Stegman et al.*, 2006; *Capitanio et al.*, 2009; *Moresi et al.*, 2014].

We do not take account the effects of a mid-oceanic ridge in the central area of the oceanic basin because we simply consider subduction of a single oceanic plate. Thus, there is no spreading center in the oceanic basin to compensate its shrinking width as it closes during DDS. We also neglect the effects of side plates and assume a strike-slip boundary between the subducting oceanic slabs and the surrounding plates. Previous studies showed that the existence of a side plate has insignificant effects on subduction if the subducting plate is a dependent plate bounded by weak zones of faults [*Yamato et al.*, 2009; *Schellart and Moresi*, 2013].

Finally, we also assume that the overriding plate is stiff enough and cannot break up in response to rollback of the subducting slabs. For this reason, the overriding plates are assumed to be 200 times more viscous than that of the upper mantle. This simplification allows us to focus on the evolution of DDS instead of deformation of these overriding plates.

3.3. Boundary Conditions

We assume that the gravitational instability between the mature oceanic plate and upper mantle causes sinking of the subducting plate during DDS, and subduction is triggered by bending tips of this plate on both sides (Figure 4). We impose free-slip velocity boundary conditions on all sidewalls and the top boundary to enable a self-consistent DDS system; for the bottom, no-slip velocity boundary conditions are used to avoid unrealistic sliding of slab along the upper-lower boundary of the mantle. Therefore, only the negative buoyancy force (slab pull) can drive the subduction of the oceanic lithosphere and induce mantle flow, and no velocity or stress is artificially exerted onto the subducting plate or the overriding plates.

The interpretation of seismic tomography and distribution of hypocenters indicate that the Molucca plate does not subduct through the 660 km discontinuity into the lower mantle (Figures 1 and 2). Although there are some high seismic velocity bodies in the lower mantle from the seismic tomography (Figure 2), they may

represent older subducted slabs. These stagnant slabs are stiff enough to act as flow barrier boundaries that hinder the penetration of the Molucca Sea plate through the upper-lower mantle discontinuity. The 660 km discontinuity is therefore assumed as an impenetrable boundary (i.e., no-slip boundary condition) at the bottom in our models, and we only consider the process of DDS above this discontinuity.

Although we control DDS during modeling by assuming different initial geometry of the bent tips of slabs, or by varying far-field boundary conditions of the overriding plates (Table 2), these simplified configurations mimic the major behaviors of the subducting slabs and overriding plates during DDS in nature, e.g., synchronous or asynchronous subduction initiation on both sides of a single plate or relative mobility/immobility of the overriding plates.

3.4. Model Design

To begin the modeling, we run an idealized reference model of symmetrical DDS (DDS_Ref), which serves as a basic model to analyze time evolution of DDS and is used for comparison with subsequent models. Key parameters of DDS_Ref are listed in Table 1. Other models are based on this reference model, and only one parameter is modified for each to investigate the influences of (1) slab width (DDS_W200, DDS_W600, DDS_W1000, DDS_W2000, DDS_Ref 2-D, DDS_30–20_2D, and DDS_200–150_2D), (2) initial geometry of bent tips of slab to mimic contrast order of subduction initiation (DDS_30–20 and DDS_150–200), (3) far-field boundary conditions and thickness of overriding plates (DDS_Fixed and DDS_CBL100), or (4) magnitude of the negative buoyancy (DDS_$\Delta\rho$40 and DDS_$\Delta\rho$80) on the evolution of DDS. The detailed descriptions are presented in Table 2 and section 4. The modeling domain is uniformly discretized by finite elements using Underworld code, with element numbers of 192 × 48 × 32 for most of the 3-D models and 192 × 48 × 64 for DDS_W2000 in direction of length, width and thickness. The according spatial resolutions are 16.7 km × 13.8 km × 31.3 km along these directions. Element numbers are 192 × 48 for 2-D models with resolutions of 16.7 km × 13.8 km.

4. Results

4.1. Reference Model of DDS

The results from the idealized symmetrical reference DDS model show four stages of subduction (Figures 5–7 and Movie S1 in the supporting information). At the beginning, subduction of oceanic plate starts on both sides (Figures 5a–5d) and then becomes self-sustaining due to gravitational instability between the mantle and oceanic plate, leading to rollback of slabs and convergence of overriding plates and arcs (Figures 5c–5h). The upper mantle escapes in direction parallel to trenches beneath the subducting plate, i.e., through toroidal flow (e.g., Figures 5f and 6). The oceanic basin between the converging plates narrows (Figure 7a), and convergence of the overriding plates is driven by a strong horizontal, inward mantle flow induced by rollback of the descending slabs. At the same time, subduction accelerates, giving rise to the first peak at ~9 Ma on the plots of convergence rate versus time (Figure 7b) and the root-mean-square velocity (v_{rms}) of the modeling domain versus time (Figure 7c).

Next, slab tips reach the discontinuity between the upper and lower mantle (Figures 5e, 5f and 6). Subduction is retarded due to obstruction at this mechanically stronger upper-lower mantle boundary (Figure 7). After this deceleration, a short period of subduction acceleration can be observed due to slight flattening of slab tips between ~9 and 12 Ma (Figures 5e, 7b and 7c). Continuous convergence then leads to final collision of the overriding plates (Figures 5g, 5h and 7d). Closure of the oceanic basin (Figure 7a), cessation of convergence (Figures 7a–7c) and abrupt increase of compressional stress at the location where collision occurs (Figure 7d) can be observed at this stage (12–13 Ma). This strong compression may result in thrusting and thickening of the oceanic crust, and intense earthquakes in the region where collision occurs. Once collision occurs, the overriding plates stop converging and are tightly bunched together (Figures 5g, 5h and 7a). Collision is immediately followed by detachment of the subducting plate, and a short-lived increase of v_{rms} at ~13 Ma can be seen in response to this detachment (Figure 7c). Finally, the oceanic plate keeps going down and lies flat at the bottom of the upper mantle after its detachment from the collided overriding plates (Figures 5i and 5j). The mantle flow induced by detachment and flattening of the oceanic lithosphere is predominantly downward (i.e., downwelling) beneath the amalgamated plates. This flow does not vanish until flattening of the entire subducted oceanic plate at the upper-lower mantle boundary is completed. The

v_{rms} declines to its minimum at the end of this stage (Figure 7c). This scenario of DDS is similar to the conceptual description by *Soesoo et al.* [1997]: DDS initiates and draws overriding plates toward each other, followed by closure of the ocean basin and detachment of slabs from the overriding plates. These slabs keep sinking until they stagnate at the bottom of upper mantle.

4.2. Width of the Subducting Plate

In general, toroidal mantle flow gives rise to a trench-parallel gradient of velocity during subduction; i.e., the rate of slab rollback diminishes near its edge and maximizes at its center, which causes bending of trenches in subduction zones [e.g., *Stegman et al.*, 2006; *Schellart et al.*, 2010; *Faccenda and Capitanio*, 2012]. Width of slabs is one of the most important controlling factors in this process. In this section, we further investigate the effects of toroidal mantle flow on DDS by varying the width of the subducting plate.

Results show that it becomes increasingly difficult for the mantle to escape, as the subducting plate gets wider. For subduction of a plate with slab width of 200 km, 600 km and 1000 km, toroidal flow develops well and allows effective escape of the trapped upper mantle (Figures 8a–8f and Movies S2 and S3). However, in the case of a slab width of 2000 km, entrapment of mantle by the subducting slabs occurs (Figures 8g and 8h). This is because once passage between the subducting slabs and the base of the upper mantle is closed, the toroidal flow becomes the only possible passway for the mantle material to escape. This horizontal, trench-parallel toroidal flow fails to develop if slabs are too wide (e.g., for a slab width of 2000 km). In this case, the mantle beneath the dome-shaped subducting slabs is trapped and space problem ensues at the final stage of DDS (Figures 8g and 8h). Furthermore, entrapment is much more likely to happen if the toroidal mantle flow is eliminated, by replacing the 3-D model of infinitely wide plates with 2-D ones (Table 2 and Figure 9). In this case, complete subduction of an oceanic plate becomes impossible because DDS will become difficult to maintain, either for symmetrical DDS (Figure 9, left column) or for asymmetrical DDS (Figure 9, middle and right columns).

4.3. Order of Subduction Initiation

In reality, it is unlikely that subduction occurs on both sides of a plate in a perfectly symmetrical way due to its complex nature, as can be observed in the Molucca Sea region. One important factor that may influence the final shape of a subducting plate is the order of subduction initiation on each side. Subduction may begin earlier on one side and thus gets faster and goes deeper than on the other side. In this study, we mimic the contrast subduction initiations on each side of a plate simply by using bent tips of slab with different initial lengths and dipping angles. The results presented in Figures 10 and 11 and Movie S4 show that subduction on the side with a larger initial dipping angle or greater length of initial bent tips is significantly faster. This is because it is easier to trigger and maintain subduction of the presubducting plate that is unstable due to gravitational instability between the plates and the underlying mantle. This easier onset of subduction further leads to a faster subsequent sinking of the slab on this side in response to stronger slab pull as it dips deeper (Figure 11). Therefore, subduction occurs in a different style with respect to the reference model: for the side with slab having a steeper dipping angle of 30° in model DDS_30–20, subduction is much faster (Figures 10c, 10d, and 11b), making this slab the first to reach bottom of upper mantle. Another side effect of this asymmetrical subduction is decrease of convergence rate and delay of collision between two overriding plates. This is a consequence of deferred subduction owing to reduced slab pull on the less dipping side (Figures 10b and 10c).

4.4. State of the Overriding Plates

The far-field boundary conditions of the overriding plate determine whether its trailing edge is fixed, and a fixed overriding plate cannot drift freely during subduction, while a free overriding plate can move passively in response to rollback of a subducting plate [*Billen*, 2008; *Schellart and Moresi*, 2013]. We design the models with a fixed or free overriding plate of different thickness to compare the resultant convergence rate and closure position of oceanic basin, as well as the morphological evolution of the downgoing slabs (Table 2). For the model with a fixed overriding plate on the left, we attach the edge of the left overriding plate onto the left sidewall, at which the velocity condition is free-slip and can prevent this overriding plate from moving freely, while the other overriding plate on the right is free to drift.

Results show that mobility of the overriding plate have significant influence on evolution of subduction system, especially shape of slabs and trenches as well as the final position of collision (Figures 12c and 12d and Movie S4). Subduction of the slab beneath a fixed overriding plate is retarded in response to

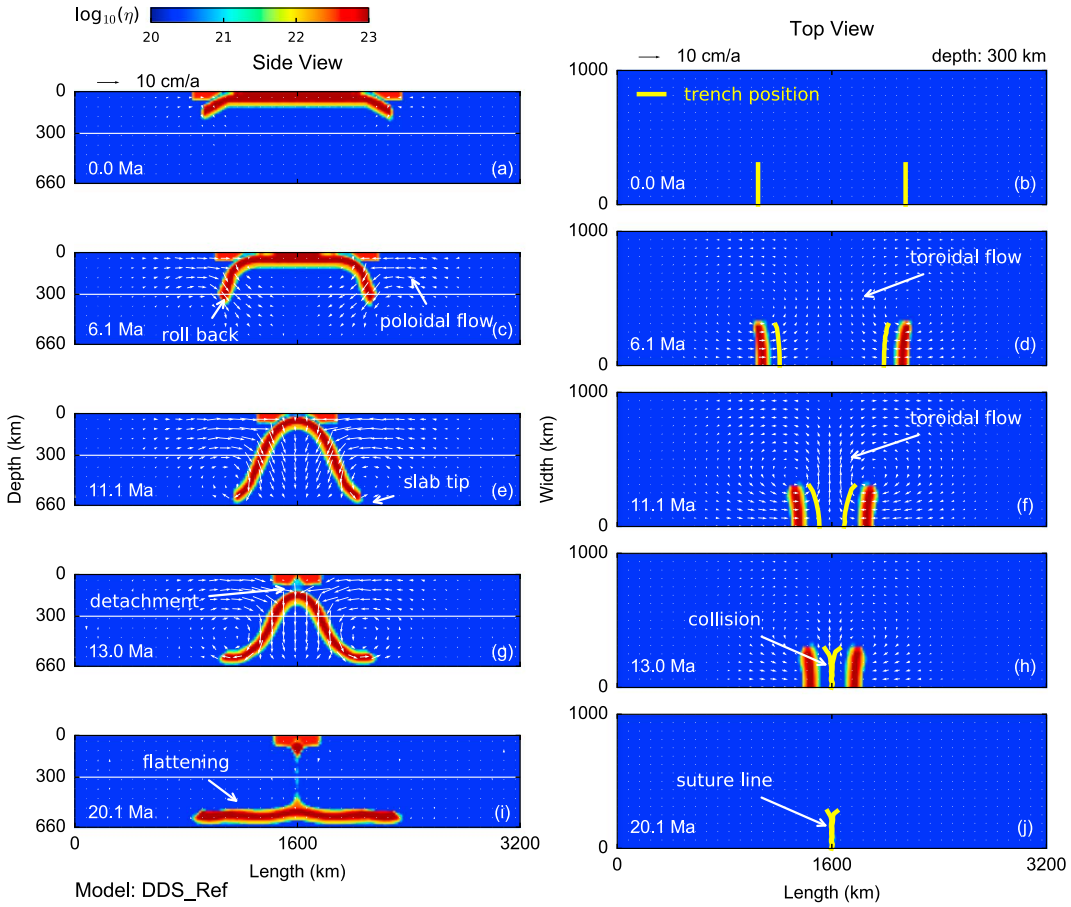

Figure 5. Time evolution of DDS at different stages. (a and b) The initial state before subduction, (c and d) free sinking of slabs and convergence of the overriding plates, and (e and f) subsequent slowing of subduction as slab tips reach the base of the upper mantle. This is followed by (g and h) collision of the overriding plates and detachment of the slab from the overriding plates and (i and j) final flattening of the entire plate at the base of the upper mantle. Vertical slices of viscosity and velocity at the central symmetry plane of slab (left column) and horizontal slices at depth of 300 km (right column) are shown. The white solid lines marks depth of the horizontal slices. Also shown is the process of trench bending in response to the toroidal mantle flow (Figures 5b, 5d, 5f, 5h, and 5j).

weakened mantle convection, which hinders descent and slab rollback (Figures 13b and 13c). Consequently, length of slab subducted beneath the fixed plate is approximately half of that beneath the free plate at 10 Ma (Figure 12c). In addition, the position of oceanic closure is shifted toward the fixed side and the space vacated by the subducted oceanic plate is mainly compensated by greater migration of the free overriding plate, making the trench more concave toward the collision position (Figures 12d and 13a). Therefore, these results suggest that the migration direction of an overriding plate can be affected by whether another overriding plate is fixed or free. This helps to explain how arc accretion and amalgamation occur during DDS: if an overriding plate is relatively fixed, it is thus more likely to "attract" the other plate to approach and is more likely to grow bigger. The competition between two (or more) major overriding plates may lead to switching of their roles from the one that "attracts" others to the one that is "attracted" by other plates, depending on whether it is free to drift.

Similarly, variation of thickness of overriding plates on both sides can also lead to formation of asymmetrical DDS. Stronger coupling between the thicker overriding plate and the subducting plates hinders subduction on this side (model DDS_CBL100; Figures 13e and 13f).

4.5. Negative Buoyancy of Oceanic Lithosphere

Gravitational instability between the oceanic lithosphere and the underlying mantle enables the occurrence of subduction of plates into interior of the Earth. This drives the tectonic movement including convergence

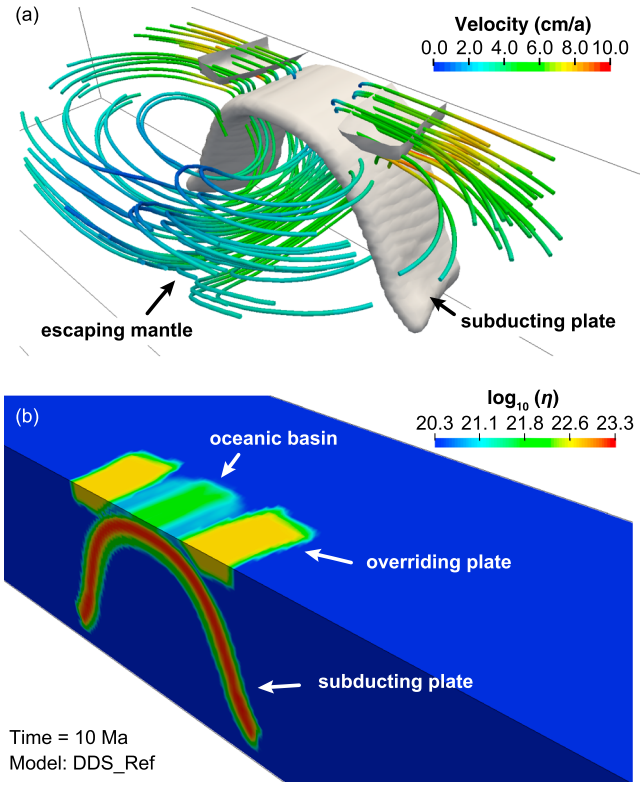

Figure 6. Oblique view the modeled DDS of the reference model DDS_Ref (at ~10 Ma) illustrating escape of the subslab mantle via rollback-induced mantle flow (also shown in Movie S1). (a) Morphology of the subducting plate (grey, defined by the isosurface of viscosity of 2.0×10^{22} Pa s) and velocity and direction of the mantle flow (colored streamlines, the color varies with velocity of the mantle flow). (b) Viscosity field viewed on different direction (shown as logarithmic value of viscosity).

and final collision between the overriding plates. In general, density contrast between the oceanic lithosphere and the surrounding upper mantle increases due to thermal contraction and eclogitization of the basaltic crust [e.g., *Cloos*, 1993; *Korenaga and Korenaga*, 2016]. Here we run extra models modified based on reference model DDS_Ref to investigate the effect of negative buoyancy on DDS by using plate with variable density contrast $\Delta\rho$ = 40, 80 kg/m^3 with respect to that of the ambient upper mantle (DDS_$\Delta\rho$40 and DDS_$\Delta\rho$80; Table 2).

The results show significant difference in subduction style between the models. The most significant observations are the contrasting time scale required for entire process of DDS (Figure 14). For models with less denser slabs ($\Delta\rho$ = 40 kg/m^3), the rates of convergence of plates and sinking of slabs are much slower with respect to that of the reference model. On the contrary, subduction of denser slabs ($\Delta\rho$ = 80 kg/m^3) leads to faster convergence owing to enhanced rollback (Figures 14a and 14b), as observed in many previous studies [e.g., *Capitanio et al.*, 2007; *Goes et al.*, 2008; *Faccenda and Capitanio*, 2012, 2013]. It is worth noting that subduction of denser slabs can lead to more intense collision between the overriding plates because of stronger rollback of slabs (Figures 14c and 14d).

5. Discussion

5.1. Symmetrical Versus Asymmetrical DDS

Dynamics of subduction of an oceanic plate can be affected by many factors, such as the size [*Stegman et al.*, 2006; *Schellart et al.*, 2007; *Duarte et al.*, 2013] and rheology [e.g., *Billen*, 2005; *Billen and Hirth*, 2007] of the subducting slabs, as well as the thickness and mobility of the overriding plate [e.g., *Capitanio et al.*, 2009; *Roda et al.*, 2011; *Rodríguez-González et al.*, 2012, 2014; *Chen et al.*, 2015; *Taramõn et al.*, 2015]. Anomaly of negative buoyancy of the subducting plate due to existence of oceanic plateaus, seamounts or mid-oceanic ridges may also complicate the stress state and the morphology of subduction zones [*Cloos*, 1993; *Niu*, 2003; *Martinod et al.*, 2005; *Liu et al.*, 2010; *Arrial and Billen*, 2013; *Moresi et al.*, 2014; *Seton et al.*, 2015]. All these factors can control the evolution of DDS in the same way. As a special form of subduction, however, DDS is further controlled by configuration of the two-subduction zones and its final shape is a competitive consequence of the double subduction.

Previous DDS models were focused on the idealized, symmetrical subduction of a plate on both sides and revealed how DDS might lead to convergence of overriding plates and the basic pattern of mantle flow that allows escape of subslab mantle [e.g., *Soesoo et al.*, 1997; *Di Leo et al.*, 2014]. Our modeling results further reveal factors that have an influence on the morphology of DDS. First, the order of subduction initiation on both sides of an oceanic plate has crucial influence on shape of the subducted plate. Relative mobility of

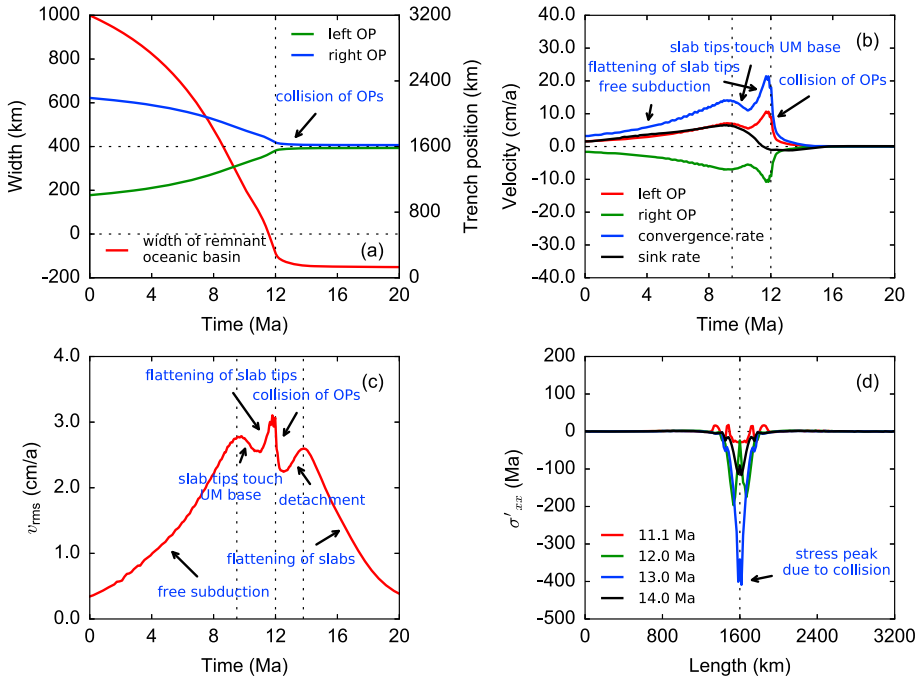

Figure 7. Key geometric and kinematic features with time during DDS for model DDS_Ref. (a) Width of the remnant oceanic basin and positions of the overriding plates showing closing of oceanic basin during convergence between the overriding plates at 0–13 Ma and collision at ~13.0 Ma. The overriding plates approach their central position and bunch together after 13.0 Ma. (b) Convergence rate of the overriding plates (red and green), closure rate of oceanic basin (blue), and sinking rate of slab tips (black) with time. (c) The root-mean-square velocity (v_{rms}) of the entire modeling domain versus time showing more details of DDS evolution than in Figure 7b: the transient speed up of mantle flow can be identified at ~14.0 Ma as the subducting plate detaches from the overriding plates before final flattening of the subducting plate. (d) Profiles of horizontal deviatoric stress σ'_{xx} with time at the center of the slab at the surface; this abnormally strong compression occurs at the fore-arc part of the overriding plates when they collide. The pulse of intense compression fades away subsequently when the slabs detach from the overriding plates. OP: overriding plate, UM: upper mantle.

the overriding plates has a similar effect and further affects in the position of final oceanic closure. In addition, the thickness of overriding plate constrains decoupling between the subducting and overriding plates and can also contribute to formation of asymmetrical DDS. To be specific, idealized DDS (e.g., simultaneous onset of subduction on both sides of an oceanic plate and free motion of overriding plates with identical thickness) results in symmetrical shape of slabs as they subduct (Figure 15a). This is rare in nature. The order of subduction initiation has crucial effect on DDS, i.e., the earlier subduction results in easier and deeper sinking of the subducted slab on one side and formation of an overall asymmetrical shape of the entire plate (Figure 15b). The relative motion of the overriding plate has a similar effect on shaping the asymmetrical DDS, because relative immobility or a larger thickness of the overriding plate leads to more difficult subduction on this side (Figures 15c and 15d). Combination and/or competition effects of these factors will result in the formation of the asymmetrical plate shape during DDS. The resultant morphology of this asymmetrical DDS depends on which effect is the overwhelming one.

The Molucca Sea plate features an asymmetrical morphology as it descends into the upper mantle (Figures 1 and 2). This plate was a micro oceanic plate isolated from the larger Philippine Sea plate during westward subduction of the Pacific plate and northward drifting of the Australian plate [*Hall*, 1996; *Knesel et al.*, 2008]. The Sangihe and Halmahera arcs were built on the bases of older arcs and had been active since the Neogene. Subduction initiated at ~20 Ma on the Sangihe side, and much later onset of subduction under the Halmahera arc is evidenced by magmatic activity that started at ~7–6 Ma, later than that of previously published age of 11 Ma [*Baker and Malaihollo*, 1996]. Subduction probably began through polarity reversal at eastern Molucca Sea plate as it collided with the other plate fragments. Afterward, the Molucca Sea plate separated from the Philippine Sea plate and became relatively independent, bordering New Guinea on its

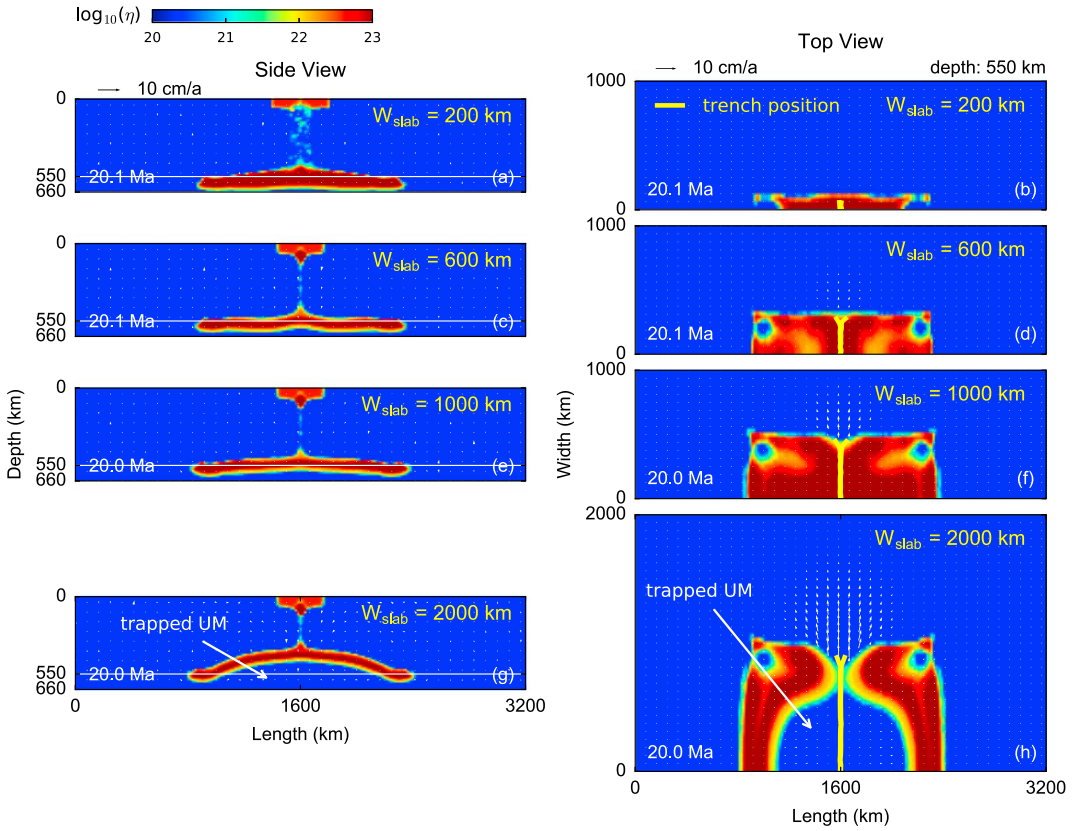

Figure 8. Effects of slab width on mantle flow for (a and b) W_{slab} = 200 km (model DDS_W200), (c and d) W_{slab} = 600 km (model DDS_W600), (e and f) W_{slab} = 1000 km (model DDS_W1000), and (g and h) W_{slab} = 2000 km (model DDS_W2000, also shown in Movies S2 and S3) at final stage of DDS (i.e., at 20 Ma). These results indicate increasing difficulty for the trapped upper mantle (UM) to escape with increasing slab width. (left column) Vertical slice at the middle symmetry plane of the slab. (right column) Horizontal slice at depth of 550 km.

south along a strike-slip fault (i.e., the Sorong Fault) and the Philippine Sea plate along the Philippine trench [*Hall and Nichols*, 1990; *Hall*, 1996]. Once initiated, subduction of the Molucca Sea plate and movement of the overriding plates led to shrinkage of the Molucca Sea and subsequent collision between the Halmahera arc and Sangihe arc since ~2 Ma [*Hall*, 1996].

Our results demonstrate that the asymmetrical morphology of the Molucca Sea plate (Figures 1b and 1c and 2b–2d) can be formed through asynchronous double subduction on both sides (Figures 10 and 12). In the Molucca Sea region, the western Sangihe arc was relatively stationary, while the eastern Halmahera arc has migrated over a large distance. It is likely that relative immobility of west overriding plate (Eurasia) might account for westward migration of the Halmahera arc (Figures 15c) and provided extensional stress required by spreading of seafloor at the Ayu Trough (Figures 1a and 3), while immobility of the Eurasian plate impedes subduction of the western Sangihe slab (Figure 15d). Similarly, relative to the Philippine Sea plate, lithosphere of the Eurasian plate is much thicker and potentially hinders subduction of the Sangihe slab (Figure 15d). Nevertheless, the observed much deeper subduction of the Sangihe slab likely reflects that the immobility and greater thickness of the Eurasian plate are subordinate to formation of the reverted U-shape configuration beneath the Molucca Sea region. Accordingly, this unique morphology of the subducted Molucca Sea plate was a predominant result of the much earlier subduction initiation on the Sangihe side (Figure 15e).

Migration and deformation of overriding plate are actually controlled by subduction-induced mantle flow, which imposes basal tractions to the overriding plates, driving their motions and internal extension due to gradient of mantle flow and compression near trench [*Duarte et al.*, 2013; *Meyer and Schellart*, 2013; *Chen et al.*, 2015]. A number of previous numerical and laboratory studies for single-sided subduction suggest

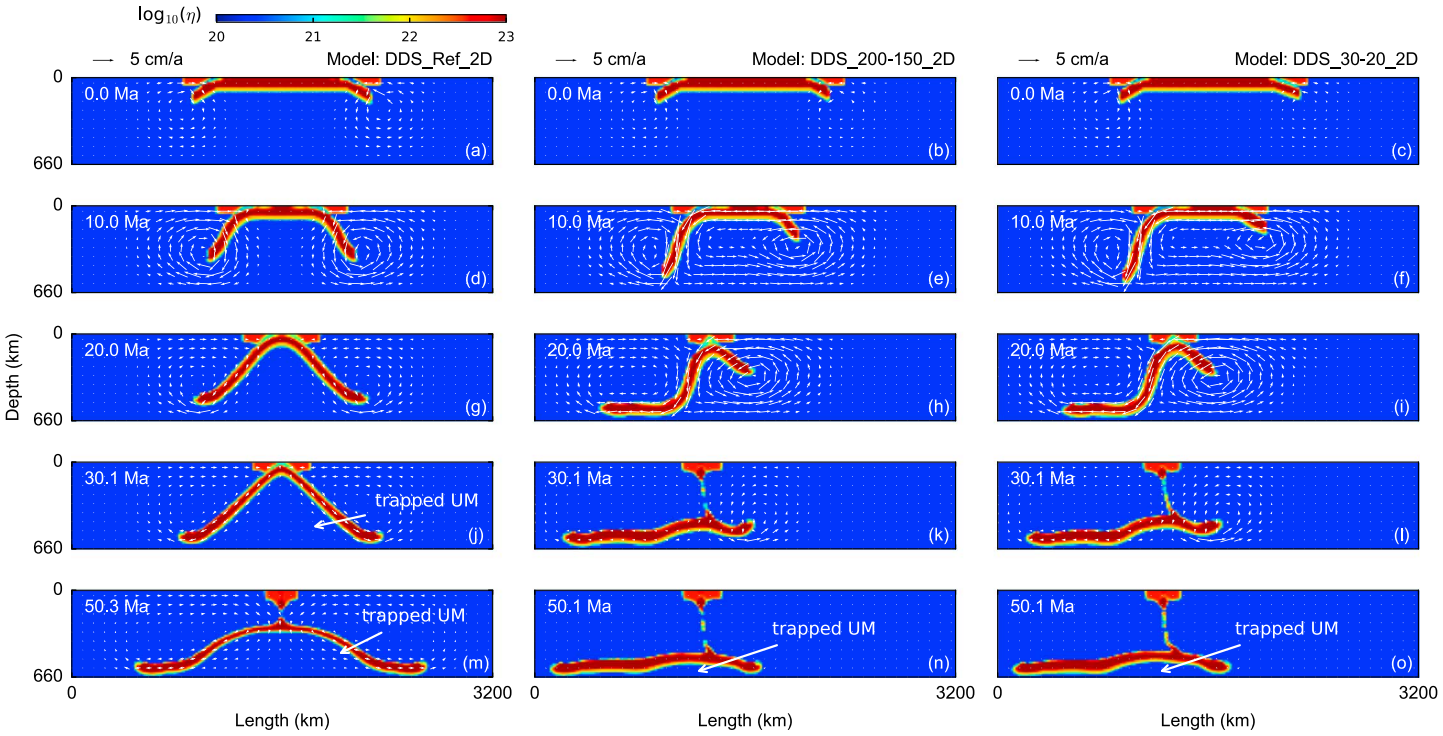

Figure 9. Results of 2-D models (left) DDS_Ref_2D, (middle) DDS_150–200_2D, and (right) DDS_30–20_2D, showing that the subslab mantle is much easier to be trapped by the subducted plate if eliminating the toroidal mantle flow. Note that the space problem is insignificant and can be overcome by lateral escape of mantle (central middle and right columns) for mantle beneath a short subducting plate (i.e., 1000 km). However, if the subducting plate is larger in length (e.g., L_{slab} = 1000 km), this lateral escape of upper mantle may always fail.

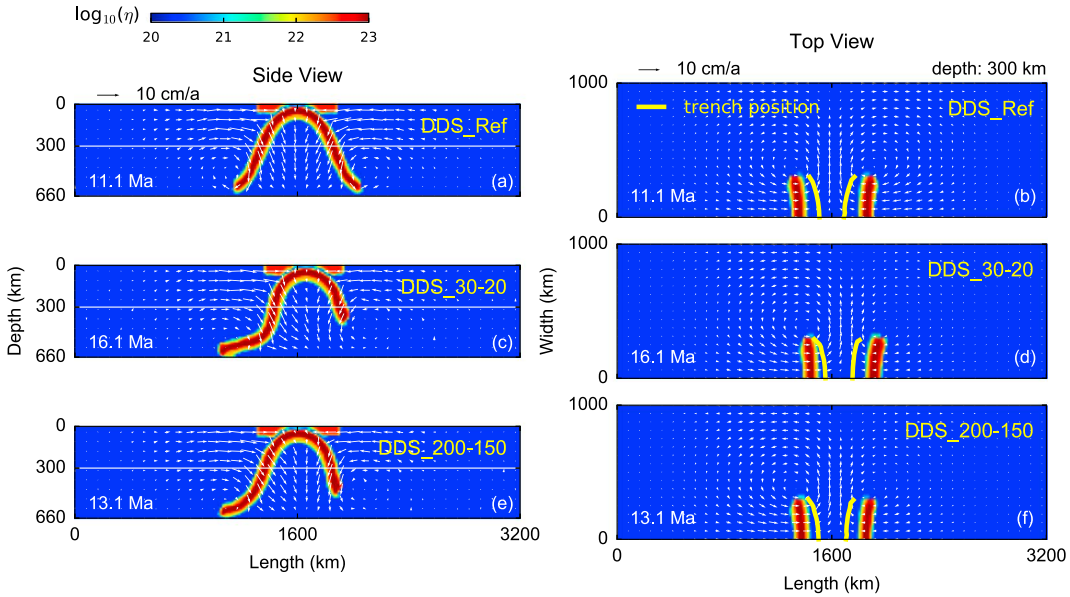

Figure 10. Comparison of DDS with different initial geometry of bent tips of slab at each side of the subducting plate. (a and b) Reference model DDS_Ref (left: φ_{pert} = 30°, L_{pert} = 200 km; right: φ_{pert} = 30°, L_{pert} = 200 km). (c and d) Model DDS_30–20 (left: φ_{pert} = 30°, L_{pert} = 200 km; right: φ_{pert} = 20°, L_{pert} = 200 km). (e and f) Model DDS_200–150 (left: φ_{pert} = 30°, L_{pert} = 200 km; right: φ_{pert} = 30°, L_{pert} = 150 km, also shown in Movie S4). These results suggest that subduction with initially shorter lengths or smaller dipping angles of the bent tip of slab yields a less active velocity field in the upper mantle and an overall asymmetrical morphology of the entire subducting plate (Figures 10c and 10e). Decrease of slab pull due to shallower dipping of slab retards subduction on this side.

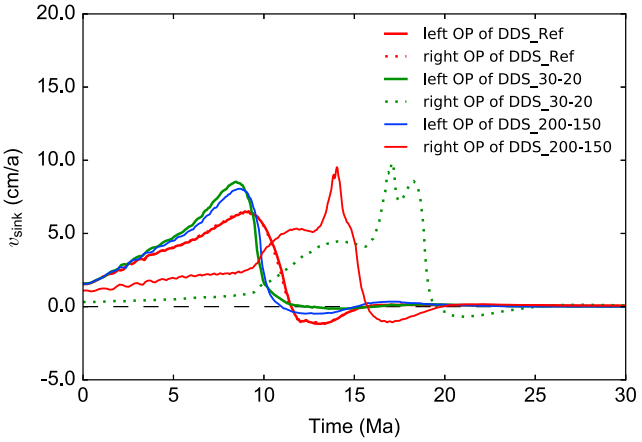

Figure 11. Sink rate of slab tips versus time for models with varied dipping angles (φ_{pert} = 30 for the left slab and φ_{pert} = 20 for the right slab) and bent tip at each side of slab (L_{pert} = 200 km for the left slab and L_{pert} = 150 km for the right slab). Contrasting kinematic features of these DDS models show that the initial geometry of bent tip has significant influence on the velocity field: faster and deeper subduction occurs on the side with longer initial bent length or greater initial slab dipping angle with respect to the other side.

that development of this concave shape of slab hinge is predominately controlled by slab width [e.g., *Stegman et al.*, 2006; *Schellart et al.*, 2010], thickness and thermal state of the overriding plates [e.g., *Meyer and Schellart*, 2013; *Rodríguez-González et al.*, 2014; *Taramón et al.*, 2015]. Our results suggest that subduction-induced mantle flow around the edges of slabs (e.g., Figure 5) was probably responsible for bending of the Halmahera and Sangihe arcs (Figure 1a). The lateral toroidal mantle flow in response to rollback of the descending Molucca Sea plate on both sides yields a variation in trench-parallel velocity, which results in faster rollback at slab center compared to that near edges of a subducting slab. The contrasting rollback velocity gives rise to bending of both the subducted slabs, and in turn bending of the trenches and arcs (Figure 16).

5.2. Driving Force of DDS and Arc Collision

Driving mechanism of plate motions has been a focus of debate in plate tectonics. As a primary force of plate movement on Earth, a direct pull generated by the subducted part of a cold oceanic plate is exerted to the rest part of plate, inducing mantle convection and dragging or pushing other plates near subduction zone [e.g., *Forsyth and Uyeda*, 1975; *Lithgow-Bertelloni and Silver*, 1998; *Schellart*, 2004; *Capitanio et al.*, 2010, 2010b, 2011]. Complex external forces are also likely to be imposed on a plate and affect the way it moves,

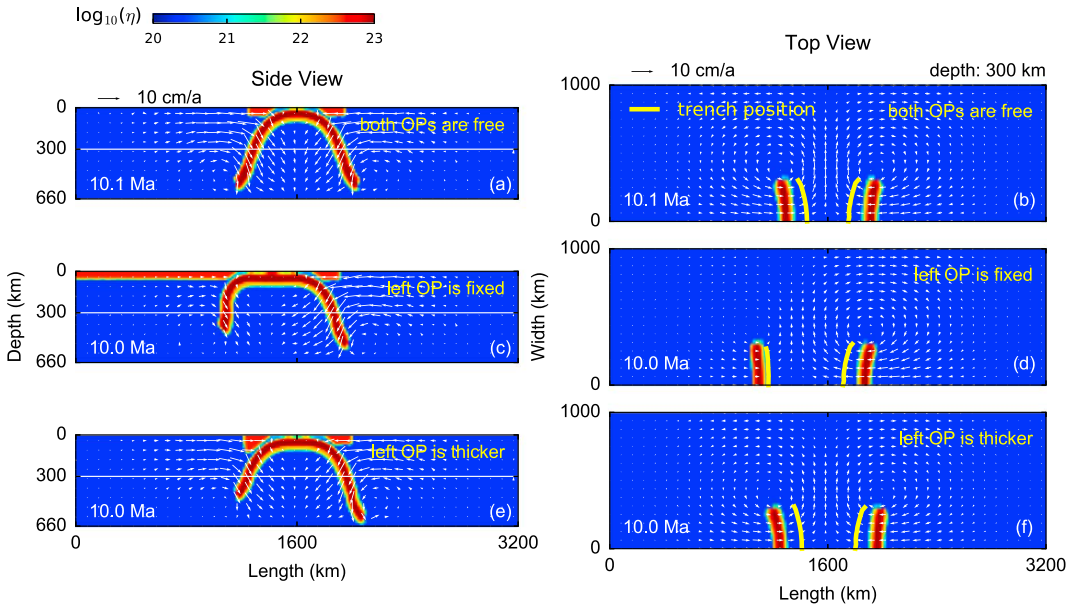

Figure 12. Comparison of DDS with (a and b) free (model DDS_Ref) and (c and d) fixed (model DDS_Fixed; Movie S5) far-field boundary velocity condition or (e and f) increased thickness (model DDS_CBL100) at left side of the overriding plate, showing contrasting slab morphology due to delayed subduction of slab beneath the a fixed or a thicker overriding plate. Also shown is the off-center of collision position at presence of the fixed overriding plate (Figures 12c and 12d).

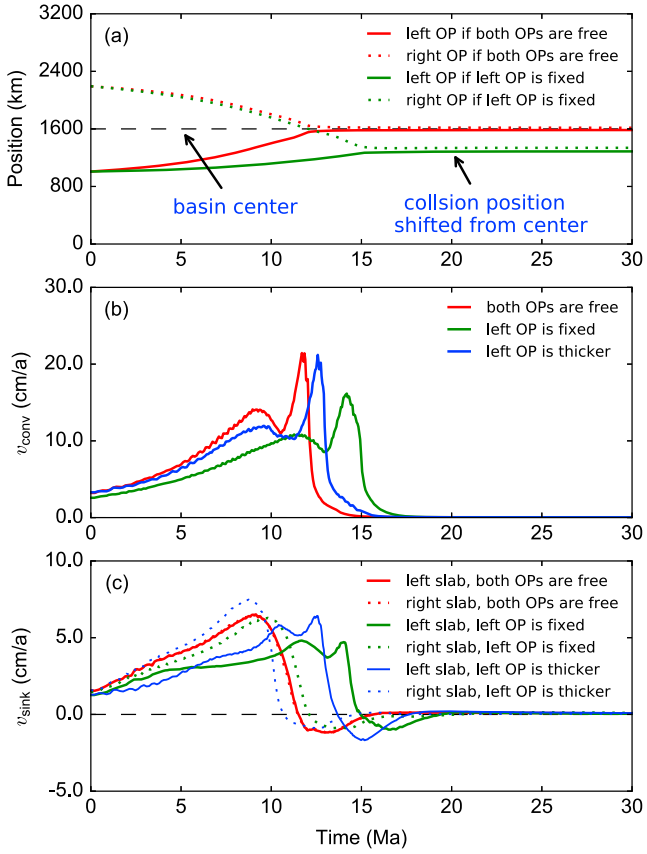

Figure 13. (a) Collision position, (b) convergence rate of the overriding plates and (c) sinking rate of slab tips for DDS model with free and fixed left overriding plate of increased thickness. Subduction of slab beneath a fixed or a thicker overriding plate is significantly slowed down (Figures 13b and 13c) and the collision deviates from the center of the oceanic basin (Figure 13a) due to contrasting convergence rate of the overriding plates (Figures 13b and 13c). OP: overriding plate.

especially for a microplate surrounded by huge ones, e.g., the Philippine Sea plate and Caroline plate [*Hall et al.*, 1995; *Gaina and Müller*, 2007].

The Molucca Sea subduction zone is characterized by collision between the Halmahera and Sangihe arcs (Figure 1), although much of SE Asia has been in an overall extensional setting during the Cenozoic [*Replumaz et al.*, 2004; *Hall*, 2012]. This collision requires force applied on the overriding Eurasian plate in the east and the Philippine Sea plate in the east, source of which remains unclear. First, it is possible that subduction of the Molucca Sea plate and arc collision were driven by the Australian plate, but tectonic reconstructions indicate that the Molucca Sea plate and the proto-Halmahera arc were situated north of the Australian plate 20 Ma ago, at least 1000 km east of its present position (Figure 3a). Therefore, the Molucca Sea plate could not have been passively squeezed toward west by the northward moving Australian plate [*Hall*, 2012]. The second possible external force was westward extrusion of the Ontong Java plateau carried by the westward drifting Pacific plate. Indentation of this massive, buoyant oceanic plateau at ~26 Ma to the trenches choked the subduction zones of the western Pacific near the equator, transmitting localized compression to the surrounding overriding plates in front of it [*Petterson et al.*, 1999; *Kerr and Mahoney*, 2007; *Knesel et al.*, 2008; *Betts et al.*, 2015; *Kufner et al.*, 2016] (Figure 3). However, seafloor spreading in the Ayu trough suggests that this area was under extension and unlikely to transmit a westward push from the indenting Ontong Java plateau to the Molucca Sea region and account for subduction of the Molucca Sea plate and the westward migration of the Halmahera arc since ~26 Ma. We can also rule out contribution of the ridge push force to the subduction of the Molucca Sea plate because the subducted Molucca Sea plate is seismologically behaving as one single plate, without signs of existence of a mid-oceanic ridge within it (e.g., Figure 2c). Another potential driving force might come from clockwise rotation of the Philippine Sea plate by an angle of about 40° since 25 Ma. This rotation might contribute a westward force on the Molucca Sea plate along its north boundary [*Baker and Malaihollo*, 1996]. Based on palaeomagnetic studies, the rotation pole was located at approximately 15°N, 150°E [*Hall et al.*, 1995] and the distance between the rotation pole and the Halmahera arc was ~2100 km, imposing a westward displacement component of ~1700 km (Figure 3). We cannot totally exclude the partial contribution of this rotation on the westward migration of the Halmahera arc, but this northwestern shear force along the northern boundary of the Molucca Sea plate should not be entirely responsible for the featured symmetrical bending of arcs during their collision (Figure 1b). In summary, it is likely that the external force was insufficient to drive subduction of the Molucca Sea plate on its both sides and the final arc-arc collision in this region.

Alternatively, the observed plate convergence and arc-arc collision in this region can be explained by self-sustaining subduction of the Molucca Sea plate. Once subduction is initiated, a mature oceanic plate

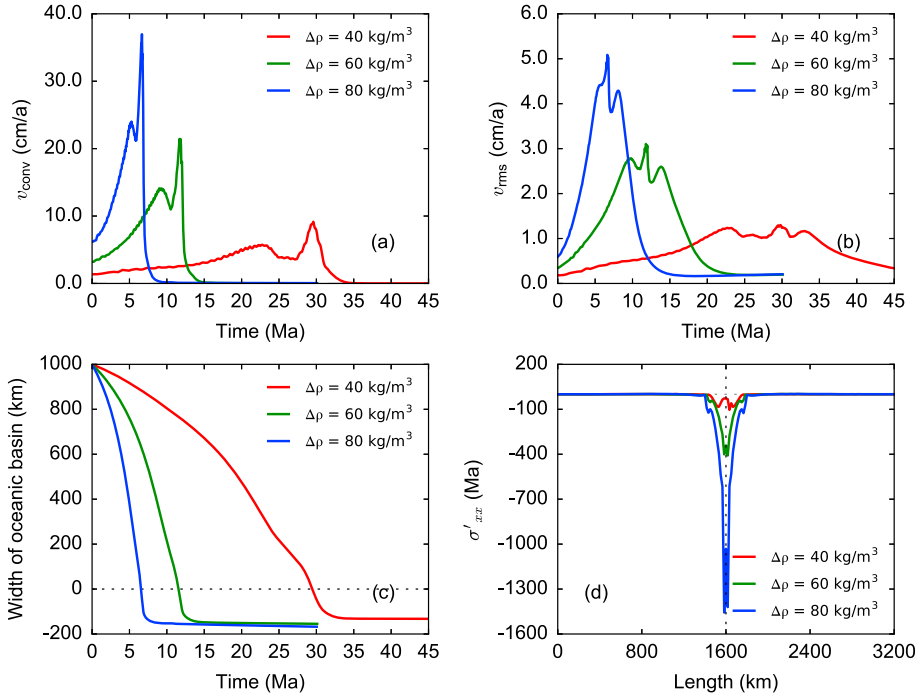

Figure 14. Influences of the negative buoyancy of slabs on evolution of DDS (models: DDS_Δρ40, DDS_Ref, DDS_Δρ80, with $\Delta\rho$ = 40, 60, 80 kg/m^3, respectively). (a) Convergence rate and (b) root-mean-square velocity, (c) width of remnant oceanic basin, and (d) surface deviatoric stress σ'_{xx} as collision of the overriding plates occurs are significantly affected by different negative buoyancy of the subducting slabs.

has sufficient negative buoyancy to maintain its subduction by the slab pull force [*Cloos*, 1993; *Korenaga and Korenaga*, 2016]. Our results show that self-consistent DDS can be solely achieved by slab pull and further leads to arc-arc collision (e.g., Figures 5, 7, and 14 and Movie S1). The rollback-induced mantle flow provides force that drives the overriding plates toward each other. Consequently, continuous DDS leads to convergence of overriding plates and collision of arcs (Figures 7a and 7d), as well as shrinkage of the oceanic basin. If so, DDS will facilitate the final closure of the oceanic basins and collision of arcs or continents in geological time. Intense earthquakes and arc magmatism are the common outcomes of DDS.

5.3. Space Problem During DDS and Its Geodynamic Implications for Plate Tectonics

DDS and other possible forms of double subduction (Figure 17) [e.g., *Maruyama et al.*, 2007; *Mishin et al.*, 2008; *Jagoutz et al.*, 2015] are relatively rare or occur only at small scales for plates of small size, and the prevailing form of plate subduction is single-sided in nature. Our modeling results of DDS provide possible explanations for this scarcity.

In general, toroidal mantle flow can give rise to a varying degree of slab rollback and trench retreat, which can be dominated by slab width [e.g., *Stegman et al.*, 2006; *Schellart et al.*, 2007, 2010]. However, we further highlight the importance of toroidal mantle flow on the geodynamics of DDS because it ensures sustainability of this type of subduction. *Soesoo et al.* [1997] realized that space problem may hinder DDS and is thus the main concern for large-scale DDS because sustainable subduction of a mature oceanic plate in the form of DDS requires effective evacuation of the slab-trapped upper mantle. Similarly, an analysis of other forms of double subduction in which two parallel subduction zones with slabs dipping in same direction (Figure 17c), suggest that narrowing of slab helped to explain acceleration of the Indian plate northward before collision with the Eurasian plate [*Billen*, 2015; *Jagoutz et al.*, 2015]. This earlier studies highlight the escape of slab-trapped mantle on geodynamics of the unusual fast migration of the Indian and close of the Tethys, whereas other authors argue that slab pull alone is insufficient to account for the rapid drift of the Indian plate. Instead, It can be driven by subduction of the Indian continent [*Capitanio et al.*, 2010], deep mantle flow [*Becker and Faccenna*, 2011], or slab pull with extra aid of external forces of the Réunion plume or ridge push [*Cande and Stegman*, 2011; *Pusok and Kaus*, 2015].

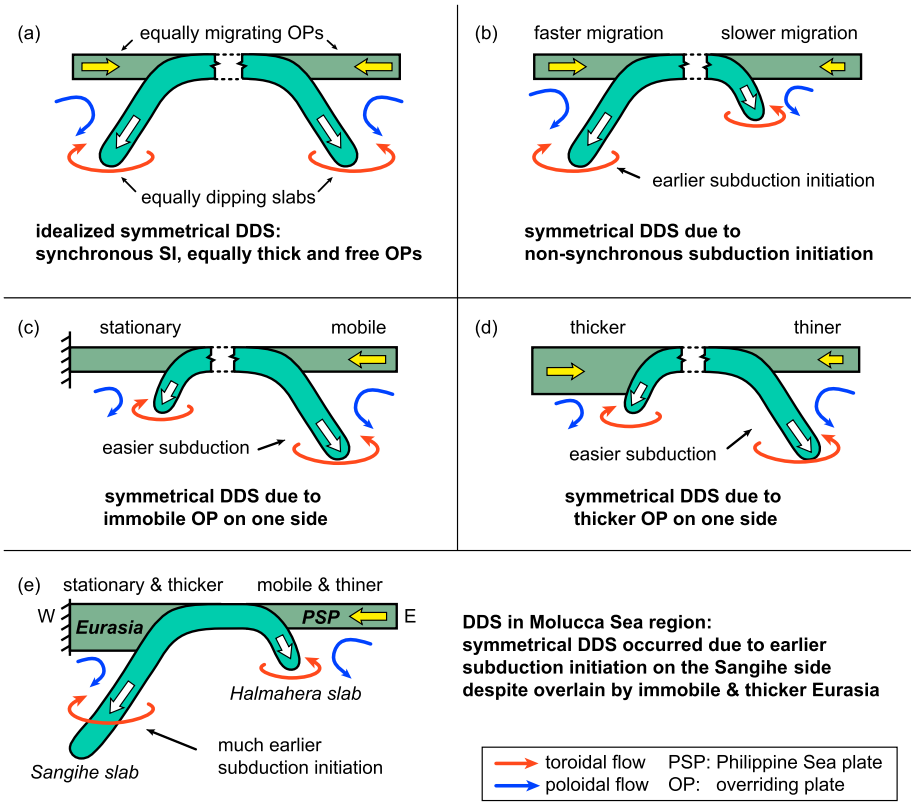

Figure 15. Cartoon of end-member models illustrating effects of the order of subduction initiation, the mobility and thickness of the overriding plates on slab morphology, and migration of the overriding plates during DDS. Idealized DDS features (a) symmetrical subduction of slabs and (b–d) asymmetrical plate shape resulted from influence of order of subduction initiation, mobility, and thickness of overriding plates, respectively. (e) Tentative interpretation of formation of the asymmetrical DDS observed in the Molucca Sea region. Size of arrows indicate relative scale of the subduction-induced mantle flow.

Previous results of 3-D numerical modeling and measurement of shear wave splitting in the Molucca Sea region reveal escape of narrow slab-trapped mantle [*Di Leo et al.*, 2012, 2014; *Li et al.*, 2014]. Our results reproduce this pattern of lateral escape of the subslab mantle (Figures 5, 6, and 8 and Movies S1–S5). With the absence of toroidal mantle flow, space problem becomes very significant and leads to difficulty in simultaneous descent of two subducting slabs and complex interplay between them [*Mishin et al.*, 2008].

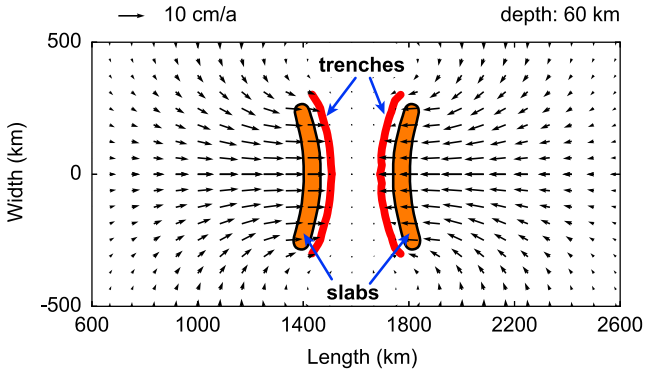

Figure 16. Tentative interpretation of arc bending due to toroidal mantle flow (top view). The positions of trenches (red) and magmatic arcs (orange) are projected to plane at depth of 60 km. The shown velocity is sliced at depth immediately beneath the overriding plates in DDS_Ref.

In addition, our 3-D modeling results confirm the difficulty of the sustained, large-scale DDS due to space problem and give specific constraint on threshold value of the maximum trench-parallel size of slab that enable successive DDS. For slab width less than ~2000 km, space problem can be overcome through effective escape of subslab mantle via toroidal flow (Figures 8a–8f). By contrast, this toroidal mantle flow is insufficient to accommodate the space between the slabs and the slab-trapped mantle when the trench-parallel size of the subducting slabs reaches or exceeds 2000 km (Figures 8g and 8h and Movies S2

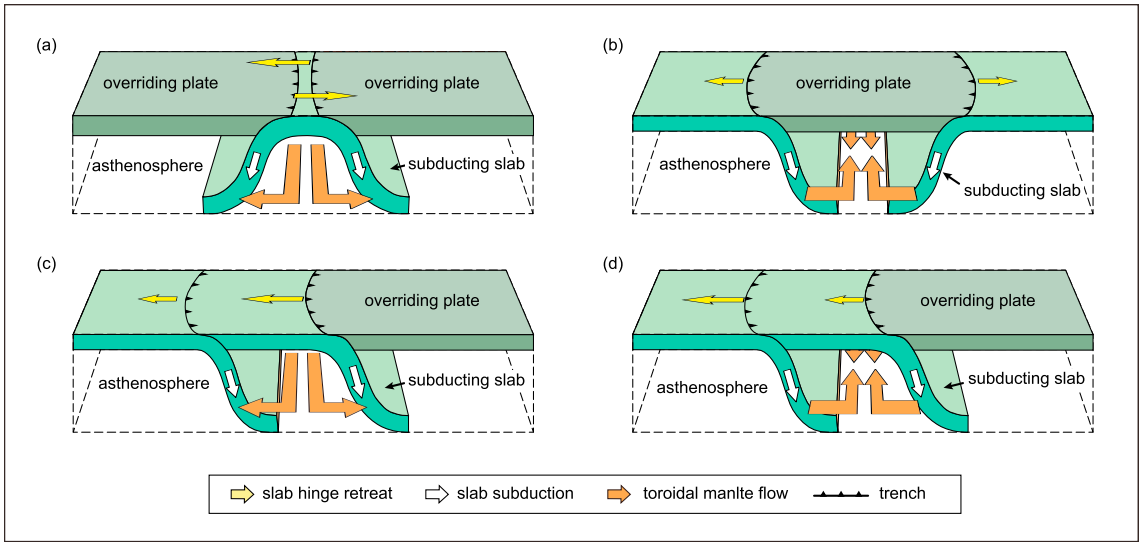

Figure 17. Cartoons illustrating several forms of double subduction. (a) Divergent double subduction (descripted in this study and by *Soesoo et al.* [1997], *Di Leo et al.* [2014], *Li et al.*, [2014], etc.). (b) Double subduction with opposite dipping directions (descripted by *Maruyama et al.* [2007]). (c and d) Convergent double subduction (descripted by *Jagoutz et al.* [2015] and *Billen* [2015]). In all of these case, sustainable subduction of the oceanic plate(s) requires smooth escape (Figures 17a and 17c) of the slab-trapped mantle or replenishment of external materials of mantle into the void space left by slab rollback (Figures 17b and 17d). The toroidal mantle flow (orange arrows) plays a dominant role in redistribution of material during all these types of double subduction.

and S3). This space problem remains even in the case of asymmetrical DDS, during which easier escape of the trapped upper mantle on the shallowly dipping side is possible (Figures 9h and 9i and Movies S4 and S5). The entrapment of mantle is thus unavoidable if the slab is too wide.

There may be several possible ways to overcome space problem during DDS in nature. First, the subducted slab is dense enough to penetrate into the lower mantle, which may partly ease the space conflict between the subducted slabs and the trapped mantle. It is also probable that tearing of the subducted slabs may occur and allow escape of the trapped mantle. In this case, subduction can no longer sustain on both sides of a plate and DDS may be transformed to ordinary single-sided subduction, which is out of the scape of this study. Finally, breakup of the oceanic plates and formation of new spreading center at mid-oceanic ridge may eliminate the space problem. In such case, the DDS cannot be maintained and is transformed into two individual single-sided subduction systems.

It is also possible that double subduction of other forms (Figures 17b–17d) encounter similar space problem. To enable smooth descent of the subducted oceanic plates into deeper mantle, large-scale lateral movement of the upper mantle is required. If the slabs are too wide, this redistribution becomes impossible due to difficulty either in escape of the trapped mantle (Figures 17a and 17c), or in inflow of mantle into gap between two subducting plates (Figures 17b and 17d). Accordingly, double subduction is not easy for a huge oceanic plate, and it can be inferred that persistent double subduction is likely confined to those oceanic slabs that are relatively narrow and short. This may explain why single-sided subduction of an oceanic slab is the dominant form for mass recycling during the Earth's evolution. In contrast, DDS may be closely associated with small oceanic plates and closure of oceanic basins of small size (e.g., the archipelagic oceans).

6. Conclusions

Collision between the Sangihe and Halmahera arcs in the Molucca Sea region and formation of the inverted U-shaped morphology of the subducting Molucca Sea plate are reproduced by 3-D numerical modeling. Our results suggest the following:

1. The self-sustaining, asymmetrical subduction of the Molucca Sea plate may drive the convergence of the overriding plates and collision of magmatic arcs, even in an extensional setting of SE Asia.
2. The earlier and faster subduction on the western Sangihe side with respect to the eastern Halmahera side predominantly led to formation of the present-day asymmetrical shape of the subducting Molucca Sea plate.

3. The relative immobility of the western overriding Eurasian plate may have promoted the westward migration of the Halmahera arc in the Molucca Sea subduction zone.
4. Bending of arcs was probably a consequence of the toroidal mantle flow induced by rollback of the subducting Molucca Sea plate on its both sides.
5. DDS is unsustainable without effective escape of the slab-trapped mantle via toroidal flow. It is therefore likely that DDS is confined to narrow and short oceanic plates and is related to closure of archipelagic oceans and accretion of arcs in accretionary orogenic belts.

Acknowledgments
This study is supported by the National Science Foundation for Outstanding Youth (grant 41525006) and the Strategic Priority Research Program (B) of Chinese Academy of Sciences (grant XDB18000000). We sincerely thank L. Moresi, L. Mondy, J. Mansour and D. Stegman for their kind help in running the Underworld code, Z.-H Li, D. Stegman, W. Schellart and P. Rey for comments and suggestions, and W. Spakman for providing the tomographic images. We are particularly grateful to R. Hall for his generous help in interpreting the tomographic data and providing information of geologic evolution in the study area as well as language polishing of the manuscript. We thank the Associate Editor F. Capitanio, M. Faccenda and another anonymous reviewer for their constructive reviews and comments, which greatly improved the manuscript. The geodynamic code Underworld [*Moresi et al.*, 2003, 2007] is available in its code repository on the GitHub website (https://github.com/underworldcode/underworld1). Free software packages Generic Mapping Tools (GMT) [*Wessel et al.*, 2013], GPlates [*Boyden et al.*, 2011] and Matplotlib [*Hunter*, 2007] are used to create the figures.

References

Amaru, M. L. (2007), Global travel time tomography with 3-D reference models, Utrecht University.
Arrial, P.-A., and M. I. Billen (2013), Influence of geometry and eclogitization on oceanic plateau subduction, *Earth Planet. Sci. Lett.*, *363*, 34–43, doi:10.1016/j.epsl.2012.12.011.
Baker, S., and J. Malaihollo (1996), Dating of Neogene igneous rocks in the Halmahera region: Arc initiation and development, *Geol. Soc. London Spec. Publ.*, *106*(1), 499–509, doi:10.1144/GSL.SP.1996.106.01.31.
Becker, T. W., and C. Faccenna (2011), Mantle conveyor beneath the Tethyan collisional belt, *Earth Planet. Sci. Lett.*, *310*(3–4), 453–461, doi:10.1016/j.epsl.2011.08.021.
Betts, P. G., L. Moresi, M. S. Miller, and D. Willis (2015), Geodynamics of oceanic plateau and plume head accretion and their role in Phanerozoic orogenic systems of China, *Geosci. Front.*, *6*(1), 49–59, doi:10.1016/j.gsf.2014.07.002.
Billen, M. I. (2005), Constraints on subducting plate strength within the Kermadec trench, *J. Geophys. Res.*, *110*, B05407, doi:10.1029/2004JB003308.
Billen, M. I. (2008), Modeling the dynamics of subducting slabs, *Annu. Rev. Earth Planet. Sci.*, *36*(1), 325–356, doi:10.1146/annurev.earth.36.031207.124129.
Billen, M. I. (2015), Geodynamics: Double dip, *Nat. Geosci.*, *8*(6), 428–429, doi:10.1038/ngeo2431.
Billen, M. I., and G. Hirth (2007), Rheologic controls on slab dynamics, *Geochem. Geophys. Geosyst.*, *8*, Q08012, doi:10.1029/2007GC001597.
Bouilhol, P., V. Magni, J. van Hunen, and L. Kaislaniemi (2015), A numerical approach to melting in warm subduction zones, *Earth Planet. Sci. Lett.*, *411*, 37–44, doi:10.1016/j.epsl.2014.11.043.
Boyden, J. A., R. D. Müller, M. Gurnis, T. H. Torsvik, J. A. Clark, M. Turner, H. Ivey-Law, R. J. Watson, and J. S. Cannon (2011), Next-generation plate-tectonic reconstructions using GPlates, in *Geoinformatics*, edited by G. R. Keller and C. Baru, pp. 95–114, Cambridge Univ. Press, Cambridge.
Cande, S. C., and D. R. Stegman (2011), Indian and African plate motions driven by the push force of the Réunion plume head, *Nature*, *475*(7354), 47–52, doi:10.1038/nature10174.
Capitanio, F. A., G. Morra, and S. Goes (2007), Dynamic models of downgoing plate-buoyancy driven subduction: Subduction motions and energy dissipation, *Earth Planet. Sci. Lett.*, *262*(1–2), 284–297, doi:10.1016/j.epsl.2007.07.039.
Capitanio, F. A., D. R. Stegman, L. N. Moresi, and W. Sharples (2009), Upper plate controls on deep subduction, trench migrations and deformations at convergent margins, *Tectonophysics*, *483*(1–2), 80–92, doi:10.1016/j.tecto.2009.08.020.
Capitanio, F. A., G. Morra, S. Goes, R. F. Weinberg, and L. Moresi (2010), India–Asia convergence driven by the subduction of the Greater Indian continent, *Nat. Geosci.*, *3*(2), 136–139, doi:10.1038/ngeo725.
Capitanio, F. A., C. Faccenna, S. Zlotnik, and D. R. Stegman (2011), Subduction dynamics and the origin of Andean orogeny and the Bolivian orocline, *Nature*, *480*(7375), 83–86, doi:10.1038/nature10596.
Capitanio, F. A., A. Replumaz, and N. Riel (2015), Reconciling subduction dynamics during Tethys closure with large-scale Asian tectonics: Insights from numerical modeling, *Geochem. Geophys. Geosyst.*, *16*, 962–982, doi:10.1002/2014GC005660.Received.
Chen, Z., W. P. Schellart, and J. C. Duarte (2015), Overriding plate deformation and variability of fore-arc deformation during subduction: Insight from geodynamic models and application to the Calabria subduction zone, *Geochem. Geophys. Geosyst.*, *16*, 3697–3715, doi:10.1002/2015GC005958.
Cloos, M. (1993), Lithospheric buoyancy and collisional orogenesis: Subduction of oceanic plateaus, continental margins, island arcs, spreading ridges, and seamounts, *Geol. Soc. Am. Bull.*, *105*(6), 715, doi:10.1130/0016-7606(1993)105<0715:LBACOS>2.3.CO;2.
Conrad, C. P. (2002), How mantle slabs drive plate tectonics, *Science*, *298*(5591), 207–209, doi:10.1126/science.1074161.
Devoti, R., C. Ferraro, E. Gueguen, R. Lanotte, V. Luceri, A. Nardi, R. Pacione, P. Rutigliano, C. Sciarretta, and F. Vespe (2002), Geodetic control on recent tectonic movements in the central Mediterranean area, *Tectonophysics*, *346*(3–4), 151–167, doi:10.1016/S0040-1951(01)00277-3.
Di Leo, J. F., J. Wookey, J. Hammond, J.-M. Kendall, S. Kaneshima, H. Inoue, T. Yamashina, and P. Harjadi (2012), Deformation and mantle flow beneath the Sangihe subduction zone from seismic anisotropy, *Phys. Earth Planet. Inter.*, *194–195*, 38–54, doi:10.1016/j.pepi.2012.01.008.
Di Leo, J. F., A. M. Walker, Z.-H. Li, J. Wookey, N. M. Ribe, J. M. Kendall, and A. Tommasi (2014), Development of texture and seismic anisotropy during the onset of subduction, *Geochem. Geophys. Geosyst.*, *15*, 192–212, doi:10.1002/2013GC005032.
Duarte, J. C., W. P. Schellart, and A. R. Cruden (2013), Three-dimensional dynamic laboratory models of subduction with an overriding plate and variable interplate rheology, *Geophys. J. Int.*, *195*(1), 47–66, doi:10.1093/gji/ggt257.
Eizenhöfer, P. R., G. Zhao, J. Zhang, and M. Sun (2014), Final closure of the Paleo-Asian Ocean along the Solonker suture zone: Constraints from geochronological and geochemical data of Permian volcanic and sedimentary rocks, *Tectonics*, *33*, 441–463, doi:10.1002/2013TC003357.
Faccenda, M., and F. A. Capitanio (2012), Development of mantle seismic anisotropy during subduction-induced 3-D flow, *Geophys. Res. Lett.*, *39*, L11305, doi:10.1029/2012GL051988.
Faccenda, M., and F. A. Capitanio (2013), Seismic anisotropy around subduction zones: Insights from three-dimensional modeling of upper mantle deformation and SKS splitting calculations, *Geochem. Geophys. Geosyst.*, *14*, 243–262, doi:10.1002/ggge.20055.
Faccenna, C., and T. W. Becker (2010), Shaping mobile belts by small-scale convection, *Nature*, *465*(7298), 602–605, doi:10.1038/nature09064.
Forsyth, D., and S. Uyeda (1975), On the relative importance of the driving forces of plate motion, *Geophys. J. R. Astron. Soc.*, *43*(1), 163–200, doi:10.1111/j.1365-246X.1975.tb00631.x.
Gaina, C., and D. Müller (2007), Cenozoic tectonic and depth/age evolution of the Indonesian gateway and associated back-arc basins, *Earth Sci. Rev.*, *83*(3–4), 177–203, doi:10.1016/j.earscirev.2007.04.004.

Gerya, T. V., and F. I. Meilick (2011), Geodynamic regimes of subduction under an active margin: Effects of rheological weakening by fluids and melts, *J. Metamorph. Geol.*, *29*(1), 7–31, doi:10.1111/j.1525-1314.2010.00904.x.
Goes, S., F. A. Capitanio, and G. Morra (2008), Evidence of lower-mantle slab penetration phases in plate motions, *Nature*, *451*(7181), 981–984, doi:10.1038/nature06691.
Gutscher, M., W. Spakman, H. Bijwaard, and E. R. Engdahl (2000), Geodynamics of flat subduction: Seismicity and tomographic constraints from the Andean margin, *Tectonics*, *19*(5), 814–833, doi:10.1029/1999TC001152.
Hall, R. (1987), Plate boundary evolution in the Halmahera region, Indonesia, *Tectonophysics*, *144*(4), 337–352, doi:10.1016/0040-1951(87)90301-5.
Hall, R. (1996), Reconstructing Cenozoic SE Asia, *Geol. Soc. London Spec. Publ.*, *106*(1), 153–184, doi:10.1144/GSL.SP.1996.106.01.11.
Hall, R. (1997), Cenozoic plate tectonic reconstructions of SE Asia, *Geol. Soc. London Spec. Publ.*, *126*(1), 11–23, doi:10.1144/GSL.SP.1997.126.01.03.
Hall, R. (2002), Cenozoic geological and plate tectonic evolution of SE Asia and the SW Pacific: Computer-based reconstructions, model and animations, *J. Asian Earth Sci.*, *20*(4), 353–431, doi:10.1016/S1367-9120(01)00069-4.
Hall, R. (2012), Late Jurassic–Cenozoic reconstructions of the Indonesian region and the Indian Ocean, *Tectonophysics*, *570–571*, 1–41, doi:10.1016/j.tecto.2012.04.021.
Hall, R., and G. J. Nichols (1990), Terrane amalgamation in the Philippine Sea margin, *Tectonophysics*, *181*(1–4), 207–222, doi:10.1016/0040-1951(90)90017-3.
Hall, R., and H. R. Smyth (2008), Cenozoic arc processes in Indonesia: Identification of the key influences on the stratigraphic record in active volcanic arcs, in *Formation and Applications of the Sedimentary Record in Arc Collision Zones*, *Geol. Soc. Am. Spec. Pap.*, *436*, edited by A. E. Draut, P. D. Clift, and D. W. Scholl, pp. 27–54.
Hall, R., and W. Spakman (2002), Subducted slabs beneath the eastern Indonesia–Tonga region: Insights from tomography, *Earth Planet. Sci. Lett.*, *201*(2), 321–336, doi:10.1016/S0012-821X(02)00705-7.
Hall, R., and W. Spakman (2015), Mantle structure and tectonic history of SE Asia, *Tectonophysics*, *658*, 14–45, doi:10.1016/j.tecto.2015.07.003.
Hall, R., J. R. Ali, C. D. Anderson, and S. J. Baker (1995), Origin and motion history of the Philippine Sea plate, *Tectonophysics*, *251*(1–4), 229–250 , doi:10.1016/0040-1951(95)00038-0.
Hinschberger, F., J. Malod, J. Réhault, M. Villeneuve, J. Royer, and S. Burhanuddin (2005), Late Cenozoic geodynamic evolution of eastern Indonesia, *Tectonophysics*, *404*(1–2), 91–118, doi:10.1016/j.tecto.2005.05.005.
Hirth, G., and D. Kohlstedt (2003), Rheology of the upper mantle and the mantle wedge: A view from the experimentalists, in *Inside Subduction Factory*, *Geophys. Monogr. Ser*, vol. 138, edited by J. Eiler, pp. 83–105, AGU, Washington, D. C.
Hunter, J. D. (2007), Matplotlib: A 2D graphics environment, *Comput. Sci. Eng.*, *9*(3), 90–95, doi:10.1109/MCSE.2007.55.
Jadamec, M. A., and M. I. Billen (2010), Reconciling surface plate motions with rapid three-dimensional mantle flow around a slab edge, *Nature*, *465*(7296), 338–341, doi:10.1038/nature09053.
Jadamec, M. A., and M. I. Billen (2012), The role of rheology and slab shape on rapid mantle flow: Three-dimensional numerical models of the Alaska slab edge, *J. Geophys. Res.*, *117*, B02304, doi:10.1029/2011JB008563.
Jagoutz, O., L. Royden, A. F. Holt, and T. W. Becker (2015), Anomalously fast convergence of India and Eurasia caused by double subduction, *Nat. Geosci.*, *8*(6), 475–U78, doi:10.1038/ngeo2418.
Ji, Y., S. Yoshioka, V. C. Manea, M. Manea, and T. Matsumoto (2016), Three-dimensional numerical modeling of thermal regime and slab dehydration beneath Kanto and Tohoku, Japan, *J. Geophys. Res. Solid Earth*, *122*, 332–353, doi:10.1002/2016JB013230.
Karato, S., and P. Wu (1993), Rheology of the upper mantle: A synthesis, *Science*, *260*(5109), 771–778, doi:10.1126/science.260.5109.771.
Kerr, A. C., and J. J. Mahoney (2007), Oceanic plateaus: Problematic plumes, potential paradigms, *Chem. Geol.*, *241*(3–4), 332–353, doi:10.1016/j.chemgeo.2007.01.019.
Knesel, K. M., B. E. Cohen, P. M. Vasconcelos, and D. S. Thiede (2008), Rapid change in drift of the Australian plate records collision with Ontong Java plateau, *Nature*, *454*(7205), 754–757, doi:10.1038/nature07138.
Korenaga, T., and J. Korenaga (2016), Evolution of young oceanic lithosphere and the meaning of seafloor subsidence rate, *J. Geophys. Res. Solid Earth*, *121*, 6315–6332, doi:10.1002/2016JB013395.
Kufner, S.-K., et al. (2016), Deep India meets deep Asia: Lithospheric indentation, delamination and break-off under Pamir and Hindu Kush (Central Asia), *Earth Planet. Sci. Lett.*, *435*(d), 171–184, doi:10.1016/j.epsl.2015.11.046.
Li, Z.-H., J. F. Di Leo, and N. M. Ribe (2014), Subduction-induced mantle flow, finite strain, and seismic anisotropy: Numerical modeling, *J. Geophys. Res. Solid Earth*, *119*, 5052–5076, doi:10.1002/2014JB010996.
Lithgow-Bertelloni, C., and P. Silver (1998), Dynamic topography, plate driving forces and the African superswell, *Nature*, *395*(6699), 345–348, doi:10.1038/26212.
Liu, L., and D. R. Stegman (2012), Origin of Columbia River flood basalt controlled by propagating rupture of the Farallon slab, *Nature*, *482*(7385), 386–389, doi:10.1038/nature10749.
Liu, L., M. Gurnis, M. Seton, J. Saleeby, R. D. Müller, and J. M. Jackson (2010), The role of oceanic plateau subduction in the Laramide orogeny, *Nat. Geosci.*, *3*(5), 353–357, doi:10.1038/ngeo829.
Martinod, J., F. Funiciello, C. Faccenna, S. Labanieh, and V. Regard (2005), Dynamical effects of subducting ridges: Insights from 3-D laboratory models, *Geophys. J. Int.*, *163*(1), 1137–1150, doi:10.1111/j.1365-246X.2005.02797.x.
Maruyama, S., Y. Isozaki, G. Kimura, and M. Terabayashi (1997), Paleogeographic maps of the Japanese Islands: Plate tectonic synthesis from 750 Ma to the present, *Island Arc*, *6*(1), 121–142, doi:10.1111/j.1440-1738.1997.tb00043.x.
Maruyama, S., M. Santosh, and D. Zhao (2007), Superplume, supercontinent, and post-perovskite: Mantle dynamics and anti-plate tectonics on the core-mantle boundary, *Gondwana Res.*, *11*(1–2), 7–37, doi:10.1016/j.gr.2006.06.003.
McCaffrey, R., E. A. Silver, and R. W. Raitt (1980), Crustal structure of the Molucca Sea collision zone, Indonesia, in *The Tectonic and Geologic Evolution of Southeast Asian Seas and Islands*, vol. 23, pp. 161–177, AGU, Washington D. C.
Meyer, C., and W. P. Schellart (2013), Three-dimensional dynamic models of subducting plate-overriding plate-upper mantle interaction, *J. Geophys. Res. Solid Earth*, *118*, 775–790, doi:10.1002/jgrb.50078.
Milsom, J. (2001), Subduction in eastern Indonesia: How many slabs?, *Tectonophysics*, *338*(2), 167–178, doi:10.1016/S0040-1951(01)00137-8.
Mishin, Y. A., T. V. Gerya, J. P. Burg, and J. A. D. Connolly (2008), Dynamics of double subduction: Numerical modeling, *Phys. Earth Planet. Inter.*, *171*(1–4), 280–295, doi:10.1016/j.pepi.2008.06.012.
Moresi, L., F. Dufour, and H.-B. Mühlhaus (2003), A Lagrangian integration point finite element method for large deformation modeling of viscoelastic geomaterials, *J. Comput. Phys.*, *184*(2), 476–497, doi:10.1016/S0021-9991(02)00031-1.
Moresi, L., S. Quenette, V. Lemiale, C. Mériaux, B. Appelbe, and H.-B. Mühlhaus (2007), Computational approaches to studying non-linear dynamics of the crust and mantle, *Phys. Earth Planet. Inter.*, *163*(1–4), 69–82, doi:10.1016/j.pepi.2007.06.009.

Moresi, L., P. G. Betts, M. S. Miller, and R. A. Cayley (2014), Dynamics of continental accretion, *Nature*, *508*(7495), 245–248, doi:10.1038/nature13033.
Morley, C. K. (2012), Late Cretaceous-early Palaeogene tectonic development of SE Asia, *Earth Sci. Rev.*, *115*(1–2), 37–75, doi:10.1016/j.earscirev.2012.08.002.
Niu, Y. L. (2003), Initiation of subduction zones as a consequence of lateral compositional buoyancy contrast within the lithosphere: A petrological perspective, *J. Petrol.*, *44*(5), 851–866, doi:10.1093/petrology/44.5.851.
Petterson, M. G., et al. (1999), Geological-tectonic framework of Solomon Islands, SW Pacific: Crustal accretion and growth within an intra-oceanic setting, *Tectonophysics*, *301*(1–2), 35–60, doi:10.1016/S0040-1951(98)00214-5.
Pownall, J. M., R. Hall, and I. M. Watkinson (2013), Extreme extension across Seram and Ambon, eastern Indonesia: Evidence for Banda slab rollback, *Solid Earth*, *4*(2), 277–314, doi:10.5194/se-4-277-2013.
Pusok, A. E., and B. J. P. Kaus (2015), Development of topography in 3-D continental-collision models, *Geochem. Geophys. Geosyst.*, *16*, 1378–1400, doi:10.1002/2015GC005732.
Puspito, N. T., Y. Yamanaka, T. Miyatake, K. Shimazaki, and K. Hirahara (1993), Three-dimensional P-wave velocity structure beneath the Indonesian region, *Tectonophysics*, *220*(1–4), 175–192, doi:10.1016/0040-1951(93)90230-H.
Rangin, C., W. Spakman, M. Pubellier, and H. Bijwaard (1999), Tomographic and geological constraints on subduction along the eastern Sundaland continental margin (South-East Asia), *Bull. Soc. Geol. Fr.*, *170*(6), 775–788.
Replumaz, A., H. Kárason, R. D. van der Hilst, J. Besse, and P. Tapponnier (2004), 4-D evolution of SE Asia's mantle from geological reconstructions and seismic tomography, *Earth Planet. Sci. Lett.*, *221*(1–4), 103–115, doi:10.1016/S0012-821X(04)00070-6.
Rey, P. F., and R. D. Müller (2010), Fragmentation of active continental plate margins owing to the buoyancy of the mantle wedge, *Nat. Geosci.*, *3*(4), 257–261, doi:10.1038/ngeo825.
Roda, M., A. M. Marotta, and M. I. Spalla (2011), The effects of the overriding plate thermal state on the slab dip in an ocean-continent subduction system, *C. R. Geosci.*, *343*(5), 323–330, doi:10.1016/j.crte.2011.01.005.
Rodríguez-González, J., A. M. Negredo, and M. I. Billen (2012), The role of the overriding plate thermal state on slab dip variability and on the occurrence of flat subduction, *Geochem. Geophys. Geosyst.*, *13*, Q01002, doi:10.1029/2011GC003859.
Rodríguez-González, J., M. I. Billen, and A. M. Negredo (2014), Non-steady-state subduction and trench-parallel flow induced by overriding plate structure, *Earth Planet. Sci. Lett.*, *401*, 227–235, doi:10.1016/j.epsl.2014.06.013.
Schellart, W. P. (2004), Kinematics of subduction and subduction-induced flow in the upper mantle, *J. Geophys. Res.*, *109*, B07401, doi:10.1029/2004JB002970.
Schellart, W. P., and L. Moresi (2013), A new driving mechanism for backarc extension and backarc shortening through slab sinking induced toroidal and poloidal mantle flow: Results from dynamic subduction models with an overriding plate, *J. Geophys. Res. Solid Earth*, *118*, 3221–3248, doi:10.1002/jgrb.50173.
Schellart, W. P., G. S. Lister, and V. G. Toy (2006), A Late Cretaceous and Cenozoic reconstruction of the Southwest Pacific region: Tectonics controlled by subduction and slab rollback processes, *Earth Sci. Rev.*, *76*(3–4), 191–233, doi:10.1016/j.earscirev.2006.01.002.
Schellart, W. P., J. Freeman, D. R. Stegman, L. Moresi, and D. May (2007), Evolution and diversity of subduction zones controlled by slab width, *Nature*, *446*(7133), 308–311, doi:10.1038/nature05615.
Schellart, W. P., D. R. Stegman, R. J. Farrington, J. Freeman, and L. Moresi (2010), Cenozoic tectonics of western North America controlled by evolving width of Farallon slab, *Science*, *329*(5989), 316–319, doi:10.1126/science.1190366.
Seton, M., et al. (2012), Global continental and ocean basin reconstructions since 200 Ma, *Earth Sci. Rev.*, *113*(3–4), 212–270, doi:10.1016/j.earscirev.2012.03.002.
Seton, M., N. Flament, J. Whittaker, R. D. Müller, M. Gurnis, and D. J. Bower (2015), Ridge subduction sparked reorganization of the Pacific plate-mantle system 60–50 million years ago, *Geophys. Res. Lett.*, *42*, 1732–1740, doi:10.1002/2015GL063057.
Silver, E. A., and J. C. Moore (1978), The Molucca Sea collision zone, Indonesia, *J. Geophys. Res.*, *83*(B4), 1681–1691, doi:10.1029/JB083iB04p01681.
Soesoo, A., P. D. Bons, D. R. Gray, and D. A. Foster (1997), Divergent double subduction: Tectonic and petrologic consequences, *Geology*, *25*(8), 755–758, doi:10.1130/0091-7613(1997)025<0755:DDSTAP>2.3.CO;2.
Stegman, D. R., J. Freeman, W. P. Schellart, L. Moresi, and D. May (2006), Influence of trench width on subduction hinge retreat rates in 3-D models of slab rollback, *Geochem. Geophys. Geosyst.*, *7*, Q03012, doi:10.1029/2005GC001056.
Stegman, D. R., R. J. Farrington, F. A. Capitanio, and W. P. Schellart (2010), A regime diagram for subduction styles from 3-D numerical models of free subduction, *Tectonophysics*, *483*(1–2), 29–45, doi:10.1016/j.tecto.2009.08.041.
Taramõn, J. M., J. Rodríguez-González, A. M. Negredo, and M. I. Billen (2015), Influence of cratonic lithosphere on the formation and evolution of flat slabs: Insights from 3-D time-dependent modeling, *Geochem. Geophys. Geosyst.*, *16*, 2933–2948, doi:10.1002/2015GC005940.
Turcotte, D. L., and G. Schubert (2014), The forces that drive plate tectonics, in *Geodynamics*, pp. 326–329, Cambridge Univ. Press, New York.
Wessel, P., W. H. F. Smith, R. Scharroo, J. Luis, and F. Wobbe (2013), Generic Mapping Tools: Improved version released, *Eos Trans. AGU*, *94*(45), 409–410, doi:10.1002/2013EO450001.
Widiyantoro, S., and R. Hilst (1997), Mantle structure beneath Indonesia inferred from high-resolution tomographic imaging, *Geophys. J. Int.*, *130*(1), 167–182, doi:10.1111/j.1365-246X.1997.tb00996.x.
Xiao, W., B. F. Windley, J. Hao, and M. Zhai (2003), Accretion leading to collision and the Permian Solonker suture, Inner Mongolia, China: Termination of the central Asian orogenic belt, *Tectonics*, *22*(6), 1069, doi:10.1029/2002TC001484.
Xiao, W., B. F. Windley, S. Sun, J. Li, B. Huang, C. Han, C. Yuan, M. Sun, and H. Chen (2015), A tale of amalgamation of three Permo-Triassic collage systems in Central Asia: Oroclines, sutures, and terminal accretion, *Annu. Rev. Earth Planet. Sci.*, *43*(1), 477–507, doi:10.1146/annurev-earth-060614-105254.
Yamato, P., L. Husson, J. Braun, C. Loiselet, and C. Thieulot (2009), Influence of surrounding plates on 3D subduction dynamics, *Geophys. Res. Lett.*, *36*, L07303, doi:10.1029/2008GL036942.
Zhao, G. (2015), Jiangnan Orogen in South China: Developing from divergent double subduction, *Gondwana Res.*, *27*(3), 1173–1180, doi:10.1016/j.gr.2014.09.004.